Using Least Squares to Construct Improved Clough-Tocher Interpolant

by

Xiang Fang

A thesis
presented to the University of Waterloo
in fulfillment of the
thesis requirement for the degree of
Master of Mathematics
in
Computer Science

Waterloo, Ontario, Canada, 2017

I hereby declare that I am the sole author of this thesis. This is a true copy of the thesis, including any required final revisions, as accepted by my examiners.

I understand that my thesis may be made electronically available to the public.

Abstract

In this thesis, a quartic Clough-Tocher interpolation scheme is introduced, and additional modifications, to adjust the macro-boundary and the order of continuity across domain triangles, are provided to improve both the mathematical and the visual quality of the resulting surface. Furthermore, a proof is given to show the convergence of the interpolation scheme under some specific constraints.

Acknowledgements

I would like to thank all people who helped me with the writing of this thesis. First, I would like to thank my supervisor Prof. Stephen Mann for his patience and support throughout the preparation of this thesis, which is impossible to exist without his guidance. Then, I would like to thank Prof. Christopher Batty and Prof. Craig Kaplan for spending their time reviewing my thesis and providing precious comments. At last, I would like to thank my family and friends for their support and encouragement.

Table of Contents

List of Figures

Chapter 1

Introduction

The objective of this thesis to improve the visual effect of interpolating surfaces. Scattered data interpolation problems study methods to construct surfaces that interpolate locations and first partial derivatives at data sites. Given data sites sampled from a specific surface, we wish to interpolate this data and build a new surface close to the original one. Often, the data sites are triangulated and spline construction schemes with Bernstein-Bézier triangular patches are used. The advantage of this scheme is that the surface is determined by a finite number of points, called control points that can be used as geometric shape handles. Also, some properties of the surface, such as tangents and continuity conditions, can be identified by the values of the control points. The shape of a surface is usually judged by the degree of mathematical smoothness, but also by its visual smoothness. For simple piecewise polynomial surfaces, the minimal degree of the Bézier patches required to meet the C^1 continuity conditions with a single polynomial patch per data triangle is five [7]. For C^2 continuity the minimum degree is nine [7]. It is desirable to reduce the degree of the Bézier patches for computational and mathematical reasons.

The degree of the interpolant can be reduced by splitting each domain triangle into multiple triangles. One of the simplest splitting schemes is the Clough-Tocher interpolant [1], which splits each triangle into three smaller ones. This scheme reduces the degree of C^1 continuous surfaces to three, and also provides an extra degree of freedom for each boundary. Kashyap gave ways to improve the interpolant's quality by adjusting the available degrees of freedom [3].

One approach to further improve the Clough-Tocher interpolant's quality is by partially increasing the order of the continuity of the surface. A major limitation of the cubic Clough-Tocher interpolants is that the boundaries of the triangles are fixed, which causes

wrinkles and bumps. The method here is to increase the degree of the scheme to achieve additional smoothness beyond C^1 continuity. For Clough-Tocher interpolants, degree seven is required for C^2 continuity [5]. In this thesis, two quartic scheme are provided. The first achieves good shape by adjusting a boundary control point, but is only C^1 across all boundaries. The second scheme provides "partial" C^2 continuity, which means the surfaces meet with at least C^1 continuity across all boundaries, and achieve C^2 continuity across some boundaries. These two schemes can be combined together, and a surface, with both good shape and C^2 continuity across some boundaries, can be obtained.

The one criterion to judge a surface's quality is its visual shape. Another criteria to judge the shape of a surface is the Gaussian curvature. I will judge and compare the smoothness of the surfaces by simple shaded images as well as the corresponding Gaussian curvature plots. While other metrics to evaluate surface quality are available, the shape defects seen in the surfaces in this thesis are severe enough that these two metrics suffice to analyze these surfaces.

1.1 Triangular Bézier Patch

The surfaces used in this thesis are triangular Bézier patches [8]. An n-th degree Bernstein-Bézier triangular patch is defined as

$$b^n(\boldsymbol{u}) = \sum_{|\boldsymbol{i}|=n} b_{\boldsymbol{i}} B^n_{\boldsymbol{i}}(\boldsymbol{u}),$$

where $B^n_{\boldsymbol{i}}(\boldsymbol{u})$ are the Bernstein polynomials,

$$B^n_{\boldsymbol{i}}(\boldsymbol{u}) = \binom{n}{\boldsymbol{i}} u^i v^j w^k,$$

with $\boldsymbol{u} = (u, v, w)$ being barycentric coordinates relative to a domain triangle. $\boldsymbol{i} = (i, j, k)$ is a multi index with $n = |\boldsymbol{i}| = i + j + k$, where $\binom{n}{\boldsymbol{i}} = \dfrac{n!}{i!j!k!}$.

The $b_{\boldsymbol{i}}$ are called *Bézier ordinates*, which form the control net of the triangular patch, as shown in Figure 1.1. In general the $b_{\boldsymbol{i}}$ are three dimensional values, and each dimension is independent from the others. However, in this thesis, all surfaces will be defined over the xy-plane, which is split into triangles formed by the xy-coordinates of $b_{(n,0,0)}$, $b_{(0,n,0)}$, and $b_{(0,0,n)}$, and in each triangle the xy-coordinates of the remaining control points are uniformly distributed. Thus the x- and y-values for each control point are fixed, so they

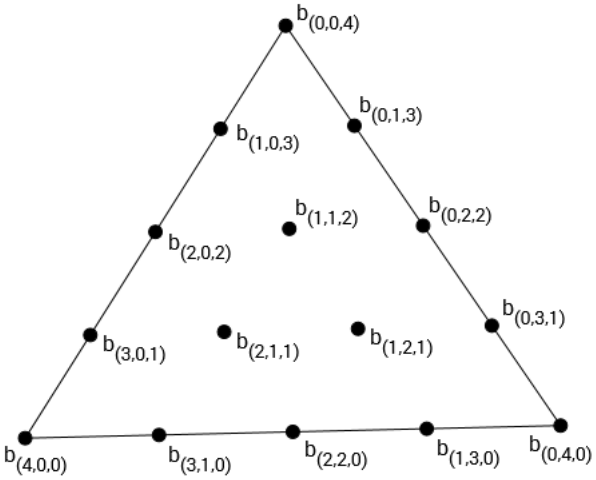

Figure 1.1: Layout of a quartic Bernstein-Bézier triangular patch

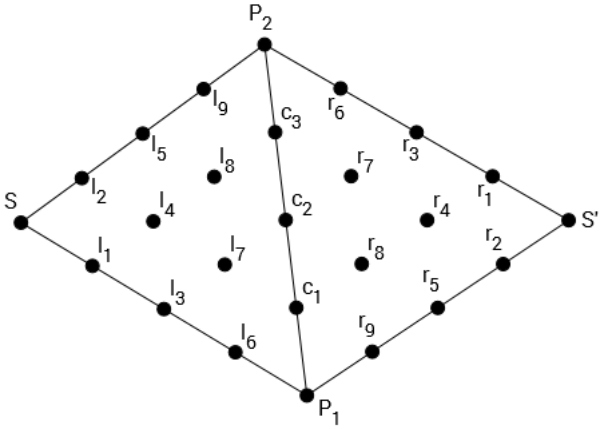

Figure 1.2: 2-D view of two adjacent patches

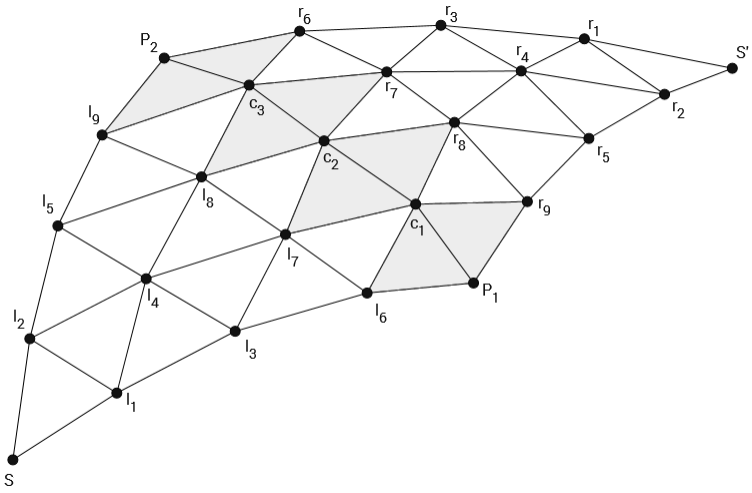

Figure 1.3: 3-D view of C^1 continuity conditions

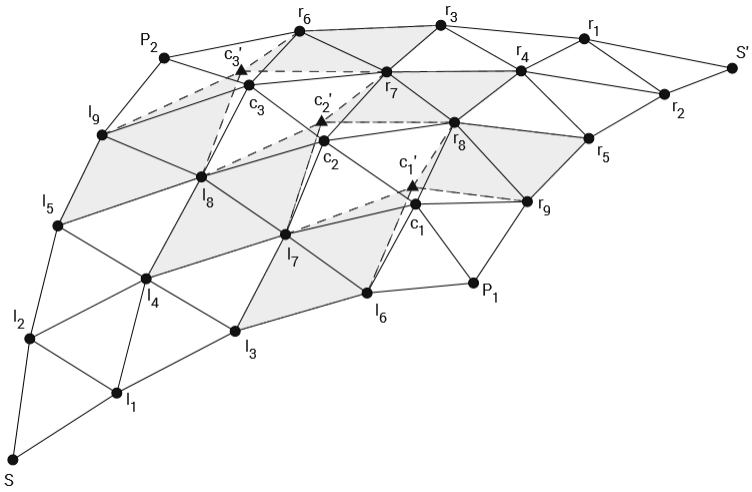

Figure 1.4: 3-D view of C^2 continuity conditions

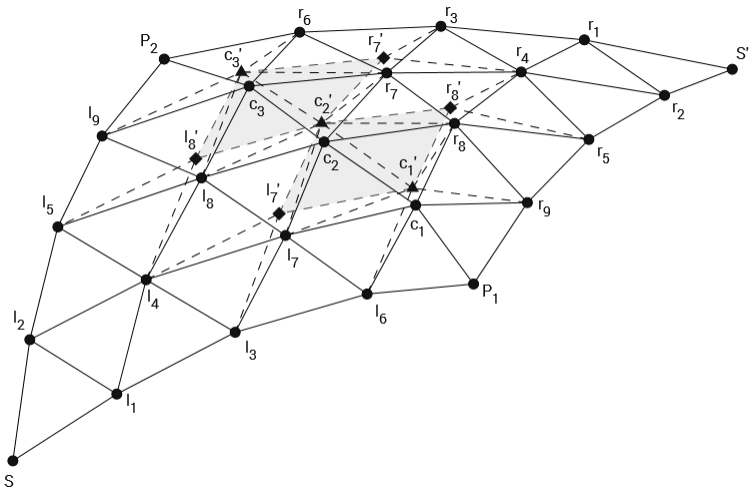

Figure 1.5: 3-D view of C^3 continuity conditions

are known in the following analyses. The value of a control point denotes the corresponding z-value of the control point.

The continuity conditions presented in this section were introduced by Lai [4]. For two triangular Bézier patches to meet with C^k continuity, their control points must satisfy certain constraints. Consider two adjacent Bézier patches as shown in Figure 1.2. Let (u, v, w) be the barycentric coordinates of S' with respect to triangle $\triangle SP_1P_2$, and let (u', v', w') be the barycentric coordinates of S with respect to $\triangle S'P_2P_1$. The patches meet with C^0 continuity if the patches share a common boundary, i.e., the boundary formed by points P_1, c_1, c_2, c_3, and P_2 in Figure 1.2. Furthermore, for the patches to meet with C^1 continuity, adjacent panels along the boundary (shown in Figure 1.3) should be coplanar. This coplanarity can be expressed algebraically as

$$\begin{aligned} r_6 &= ul_9 + vc_3 + wP_2 \\ r_7 &= ul_8 + vc_2 + wc_3 \\ r_8 &= ul_7 + vc_1 + wc_2 \\ r_9 &= ul_6 + vP_1 + wc_1. \end{aligned} \tag{1.1}$$

If the C^1 condition is satisfied, then Figure 1.4 illustrates an additional condition required for C^2 continuity: each pair of extension points obtained by the shaded panels (triangular

points) should be equal:

$$\begin{array}{rcccl} c_1' & = & ul_3 + vl_6 + wl_7 & = & u'r_5 + v'r_8 + w'r_9 \\ c_2' & = & ul_4 + vl_7 + wl_8 & = & u'r_4 + v'r_7 + w'r_8 \\ c_3' & = & ul_5 + vl_8 + wl_9 & = & u'r_3 + v'r_6 + w'r_7. \end{array} \tag{1.2}$$

The additional conditions to achieve C^3 continuity are illustrated in Figure 1.5: each shaded pair of adjacent triangles formed by the second level extension points (triangular points) and the third level extension points (diamond points) should be coplanar. The values of the third level extension points can be expressed as

$$\begin{array}{rcl} l_7' & = & ul_1 + vl_3 + wl_4 \\ l_8' & = & ul_2 + vl_4 + wl_5 \\ r_7' & = & u'r_1 + v'r_3 + w'r_4 \\ r_8' & = & u'r_2 + v'r_4 + w'r_5, \end{array}$$

and the C^3 conditions are

$$\begin{array}{rcl} r_7' & = & ul_8' + vc_2' + wc_3' \\ r_8' & = & ul_7' + vc_1' + wc_2'. \end{array} \tag{1.3}$$

Furthermore, for our purposes, if these conditions of continuity are not satisfied, the difference between each side of equations (1.1), (1.2), and (1.3) will be used to represent the discontinuity of each order.

1.2 Clough-Tocher Interpolant

For a given triangulation of data sites with z-values and first partial derivatives, it is impossible, in general, to construct a C^1 piecewise Bézier triangular interpolant using one cubic Bézier patch per data triangle. For cubic patches, the number of control points is not enough to satisfy the continuity conditions across all boundaries. To avoid this, there are two methods that can be applied: increase the degree of the Bézier patches, or split the domain triangles. The Clough-Tocher interpolants were invented to solve these kinds of scattered data interpolation problems. This scheme divides each domain triangle (called *macro-triangles*) into three smaller ones (called *mini-triangles*), and fits a cubic triangular Bézier patch in each mini-triangle, where the patches interpolate the positions and normals at the data sites and meet each other with C^1 continuity.

The layout of the control points in the split triangles are shown in Figures 1.6 and 1.7. The bold lines denote the macro boundaries across macro-triangles and the thin lines

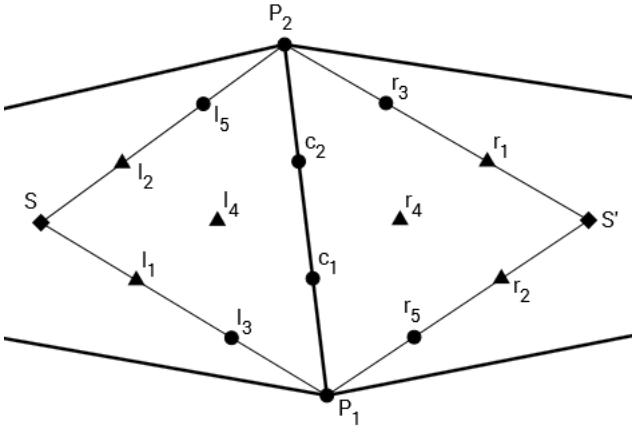

Figure 1.6: An exterior boundary across macro triangles

- Type A control points.
- ▲ Type C control points.
- ⧫ Type E control points.

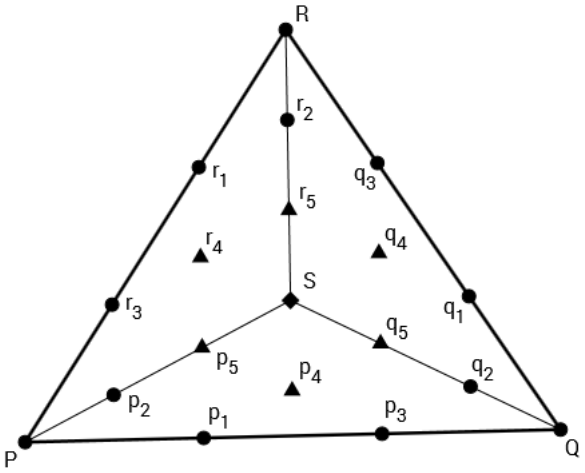

Figure 1.7: Interior boundaries inside a macro triangle

- Type A control points.
- ▲ Type C control points.
- ⧫ Type E control points.

denote interior boundaries. For convenience, these control points are classified into three categories:

Type A:	$P_1, P_2, l_3, l_5, r_3, r_5, c_1, c_2$ in Figure 1.6,
	$P, Q, R, p_1, p_2, p_3, q_1, q_2, q_3, r_1, r_2, r_3$ in Figure 1.7.
Type C:	$l_1, l_2, l_4, r_1, r_2, r_4$ in Figure 1.6,
	$p_4, p_5, q_4, q_5, r_4, r_5$ in Figure 1.7.
Type E:	S, S' in Figure 1.6,
	S in Figure 1.7.

The choice of 'A', 'C', and 'E' was made to better match the type of quartic control points in Chapter 3. Initially, the the values of all control points are undetermined. The construction proceeds as follows:

1. The values of the type A control points can be set by the location and tangent values of the data sites.

2. Proper values are chosen for control points l_4 and r_4 in Figure 1.6, such that control points l_4, c_1, r_4, and c_2 are coplanar.

3. In Figure 1.7, the values of control points p_5, q_5 and r_5 can be determined by locating them on the planes spanned by $\triangle p_2 p_4 r_4$, $\triangle q_2 q_4 p_4$, and $\triangle r_2 r_4 q_4$, respectively.

4. The value of S can be determined by locating it on the plane of $\triangle p_5 q_5 r_5$.

The resulting patches interpolate the data, and the neighbouring patches meet with C^1 continuity.

Figure 1.8 shows the Franke's function No.1, which will be used as the testing source in this thesis. All examples provided in this thesis are built over the region $[0.0, 1.0] \times [0.0, 1.0]$ with a 4×4 regular network, on which all points and tangents are sampled from the Frank's function No.1 [2]:

$$\begin{aligned} f(x,y) \;=\; & 0.75e^{-\frac{(9x-2)^2+(9y-2)^2}{4}} \\ & +0.75e^{-\frac{(9x+1)^2}{49}-\frac{(9y+1)^2}{10}} \\ & +0.5e^{-\frac{(9x-7)^2+(9y-3)^2}{4}} \\ & -0.2e^{-(9x-4)^2-(9y-7)^2}. \end{aligned}$$

In the curvature plots, red denotes positive curvature, blue denotes negative curvature, and green denotes zero curvature.

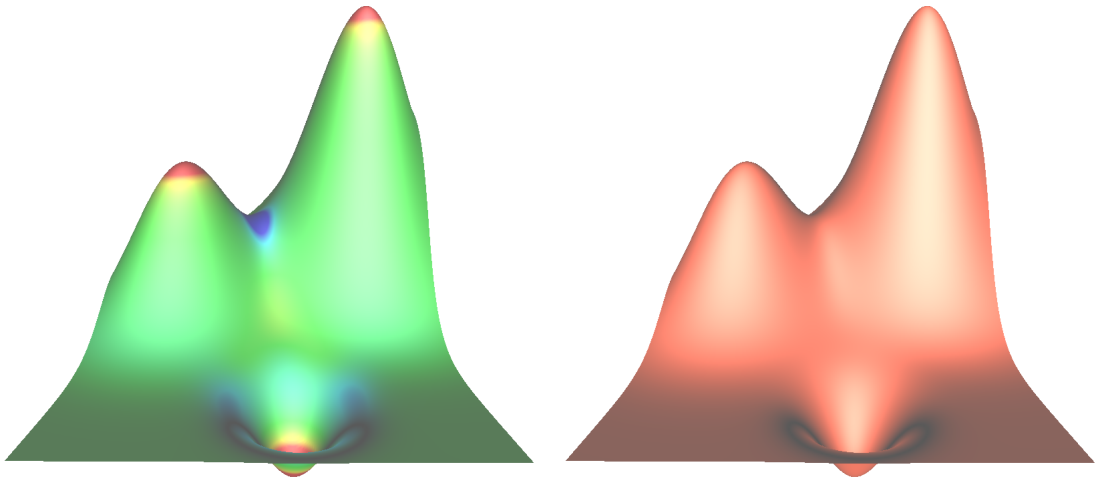

Figure 1.8: Franke's Function No.1

Figure 1.9 shows the cubic surface constructed by the original Clough-Tocher algorithm. Abrupt changes in curvature can be seen in the curvature plot, and major shape defects are apparent in the shaded image even though the patches meet with C^1 continuity.

1.3 Least Squares

This thesis will use least squares to improve the surface quality. Least squares minimizes the error between a group of known values $l_1, l_2, l_3, \ldots, l_n$ and a group of dependent unknown values $r_1, r_2, r_3, \ldots, r_n$ by minimizing the sum of the squares of the difference between each pair:

$$\min \sum_{i=1}^{n} (l_i - r_i)^2. \tag{1.4}$$

In general, this equation can be minimized by taking its derivative with respect to r_i and setting it to zero. Square values are used in Equation (1.4) since taking its derivative results in a system of linear equations. The solution to the resulting linear equation gives the values of the r_i that minimize Equation (1.4).

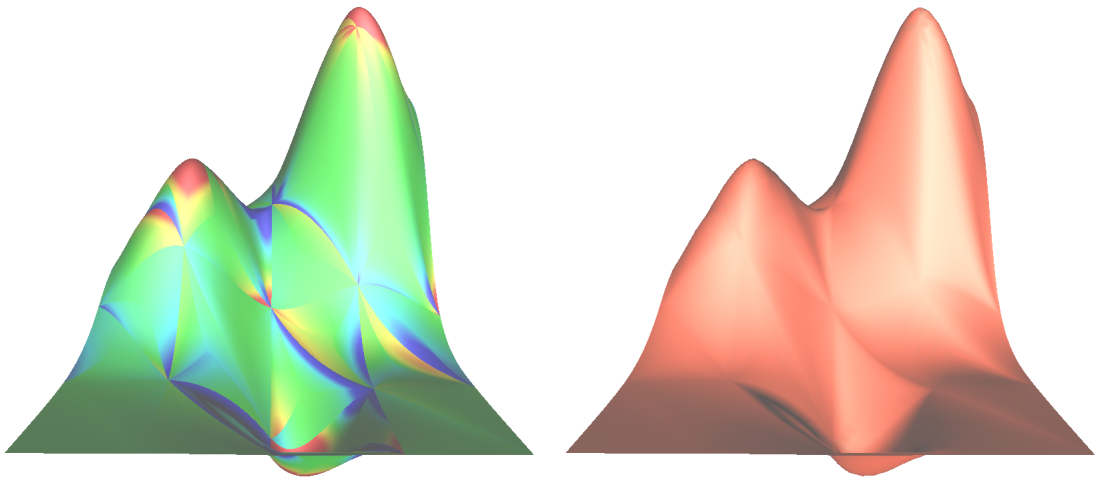

Figure 1.9: The curvature plot (left) and the shaded image (right) of the cubic surface provided by the original Clough-Tocher algorithm

Chapter 2

Improved Cubic Clough-Tocher Interpolants

The original Clough-Tocher scheme used cubic Bézier patches, which have an extra degree of freedom for the center control points. Several algorithms were developed to adjust the center control points to get better shaped interpolants. In this section, improved Clough-Tocher schemes provided by Kashyap [3] will be reviewed.

Recall that the control points of cubic Bézier patches are distributed uniformly in the xy-plane. The layout of the control points are shown in Figures 1.6 and 1.7. The values of the center control points (l_4 and r_4 in Figure 1.6, and p_4, q_4, and r_4 in Figure 1.7) need to be determined, and then the values of the other control points can be determined by the values of these center control points.

In addition to a cubic precision variant, the strategies used in this chapter are fairing algorithms, which includes exterior fairing across the macro-boundaries and interior fairing across the interior boundaries. Exterior fairing and interior fairing will be applied repeatedly. Each operation minimizes or eliminates a specific order of discontinuity while maintaining the conditions of a lower order continuity. For the cubic case, the C^2 discontinuity is minimized with the C^1 conditions satisfied. I will use similar fairing strategies in Chapter 3 for a quartic version of the Clough-Tocher scheme.

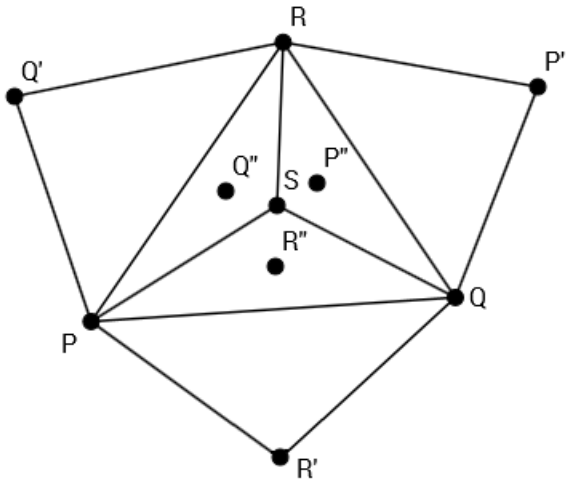

Figure 2.1: A split macro-triangle and its neighbour vertices

2.1 Cubic Precision Center Control Points

The first method is to choose values for the center control points of each Bézier patch so that the patches have cubic precision. An interpolation algorithm has n-th degree precision if the interpolant reproduces a degree n polynomial F, when the input data is sampled from F. If a surface has higher order of precision, it will be a better approximation to the sampled target.

As shown in Figure 2.1, $\triangle PQR$ is a macro-triangle split at S and P' is a neighbour vertex. An initial value of the center control point P'' will be determined by the values of P, Q, R, and P'. First fit a single cubic triangular Bézier patch to $\triangle PQR$ with respect to the location and tangent of P, Q, and R. There exists one degree of freedom. Now, force the surface to interpolate the location of P' (ignore its tangent). The patch that interpolates this data is unique. Finally, subdivide the patch at S into three smaller patches, and use the value of the center control point of patch over $\triangle SQR$ as the value of P''. Similar analyses can be applied to the other two points Q' and R' to set Q'' and R''.

If the input data at P, Q, R, P', Q', and R' are sampled from a cubic function, then this scheme will reproduce that cubic surface [6]. The patches will meet C^∞ since they represent the same function. If not, the result is still better than the original Clough-Tocher scheme.

Figure 2.2 shows the difference between the cubic surfaces provided by the original and

the cubic precision Clough-Tocher algorithms. As can be seen, the cubic precision surface is smoother, although it still has significant shape artifacts.

2.2 Exterior Fairing

Kashyap gave the following method to fair across the macro-boundaries, basically by minimizing the C^2 discontinuity between them. In Figure 1.6, let (u, v, w) be the barycentric coordinates of S' with respect to $\triangle SP_1P_2$, and let (u', v', w') be the barycentric coordinates of S with respect to $\triangle S'P_2P_1$. Consider the values of the center control points: the values of l_4 and r_4 are needed to satisfy the conditions

$$ul_4 + vc_1 + wc_2 = r_4 \tag{2.1}$$

to meet with C^1 continuity, and from (1.2) the C^2 discontinuity across the macro-boundary can be represented in least squares form:

$$\begin{aligned}(ul_1 + vl_3 + wl_4 - u'r_2 - v'r_4 - w'r_5)^2 \\ +(ul_2 + vl_4 + wl_5 - u'r_1 - v'r_3 - w'r_4)^2.\end{aligned} \tag{2.2}$$

To satisfy (2.1), substitute the value of r_4 from (2.1) into the C^2 discontinuity formula (2.2), take the first derivative with respect to l_4 or r_4, and set it to be zero. The solution to this least square problem gives the following values for l_4 and r_4:

$$\begin{aligned} l_4 &= \frac{v(u'r_1 + v'r_3 - ul_2 - wl_5) + w(u'r_2 + w'r_5 - ul_1 - vl_3)}{2v^2 + 2w^2} - \frac{vc_1 + wc_2}{2u} \\ r_4 &= \frac{uv(u'r_1 + v'r_3 - ul_2 - wl_5) + uw(u'r_2 + w'r_5 - ul_1 - vl_3)}{2v^2 + 2w^2} + \frac{vc_1 + wc_2}{2}. \end{aligned} \tag{2.3}$$

2.3 Interior Fairing

Kashyap also gave the following method to fair across the interior boundaries. The method used for minimizing the C^2 discontinuity across exterior boundaries cannot be applied on the interior boundaries because the three center control points are pairwise associated and cannot be updated individually. Instead, Kashyap used another scheme: force the corresponding extension points to be equal, while minimizing the movement of the varying control points from their present location. Thus, starting from an initial surface, this

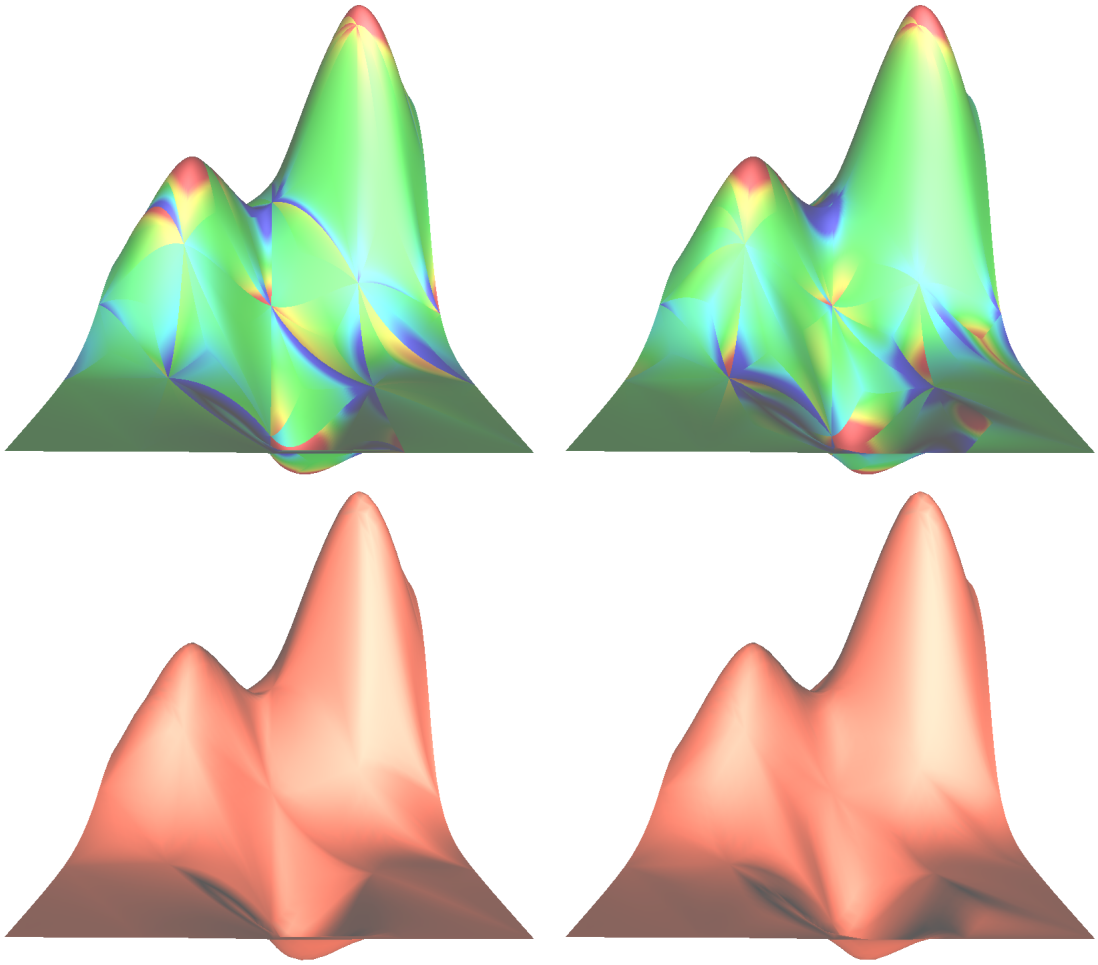

Figure 2.2: The difference between the cubic surfaces provided by the original (left) and the cubic precision (right) Clough-Tocher algorithms

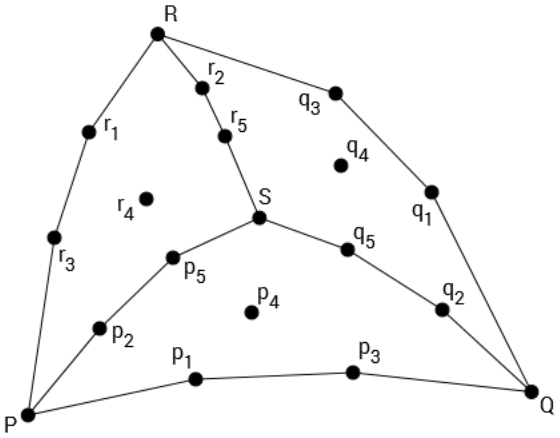

Figure 2.3: 3-D view of continuity conditions of a split macro-triangle: the layout of control points

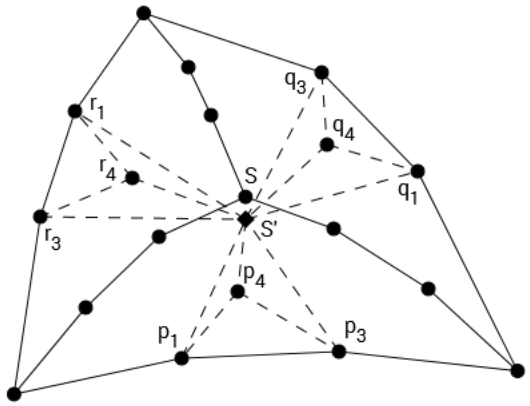

Figure 2.4: 3-D view of continuity conditions of a split macro-triangle: the C^2 continuity condition

scheme will make the patches meet with C^2 continuity and change the initial surface the least.

As shown in Figure 1.7 and Figure 2.3, S is the center of domain $\triangle PQR$. The process of the original Clough-Tocher scheme ensures that the C^1 conditions are always satisfied. Then, to achieve C^2 continuity across mini-triangle boundaries, the corresponding extension points of triangles must have the same value. For example, since S is the center of $\triangle PQR$ on the xy-plane, $S = (P+Q+R)/3$, thus $Q = -R-P+3S$ and $P = -Q-R+3S$. Thus, the barycentric coordinates of Q, with respect to $\triangle RPS$, and the barycentric coordinates of P, with respect to $\triangle QRS$, are $(-1,-1,3)$. So to achieve C^2 continuity across the interior boundary RS (Equation (1.2)), the conditions

$$\begin{aligned} -r_1 - r_3 + 3r_4 &= -q_1 - q_3 + 3q_4 \\ -r_4 - p_2 + 3p_5 &= -q_2 - q_4 + 3q_5 \end{aligned}$$

must be satisfied. Notice that the three extension points of the first condition for all three interior boundaries are all the same. Furthermore, the second condition is always satisfied since both sides are equal to the value of p_4 by the C^1 continuity conditions. Thus, as shown in Figure 2.4, the conditions of C^2 continuity on the interior boundaries are

$$\begin{aligned} S' &= 3p_4 - p_1 - p_3 \\ &= 3q_4 - q_1 - q_3 \\ &= 3r_4 - r_1 - r_3. \end{aligned}$$

This condition is always satisfiable, and the value of S' is not unique. Kashyap applied least squares here to obtain the value of S' that minimizes the the movement of p_4, q_4, and r_4. Let $\bar{p}$ denote the original value of point p, then the least squares equation is

$$(p_4 - \bar{p}_4)^2 + (q_4 - \bar{q}_4)^2 + (r_4 - \bar{r}_4)^2, \tag{2.4}$$

subject to the constraint of the C^2 continuity condition

$$3p_4 - p_1 - p_3 = 3q_4 - q_1 - q_3 = 3r_4 - r_1 - r_3. \tag{2.5}$$

The solution of this constrained least square problem ((2.4) with constraint (2.5)) is

$$\begin{aligned} S' &= \bar{p}_4 + \bar{q}_4 + \bar{r}_4 - (p_1 + p_3 + q_1 + q_3 + r_1 + r_3)/3 \\ p_4 &= (S' + p_1 + p_3)/3 \\ q_4 &= (S' + q_1 + q_3)/3 \\ r_4 &= (S' + r_1 + r_3)/3. \end{aligned} \tag{2.6}$$

Using these values of p_4, q_4, and r_4, we then use standard Clough-Tocher to update the values of p_5, q_5, r_5, and S.

Now there are fairing algorithms for both the exterior and interior boundaries. Kashyap applied them, in turn, several times to obtain a new surface. However, as will be discussed later, if we apply these two algorithms, in turn, an infinite number of times, the surface will switch between two stable states instead of one, i.e., the process does not converge to a single surface. Thus, the algorithm cannot meet the conditions of C^1 continuity across macro-boundaries and the C^2 continuity conditions across the interior boundaries at the same time. Algorithm 1 shows the process of Kashyap's Clough-Tocher interpolant.

Set the type A control points by the locations and derivatives of vertices to achieve C^1 continuity around vertices;
Set the type C control points by the cubic precision Clough-Tocher scheme described in Section 2.1;
Set the type E control points to achieve C^1 continuity across the interior boundaries;
// **Kashyap's fairing steps repeat**
  Update the values of l_4 and r_4 as described in Equation 2.3;
  Update the values of p_4, q_4 and r_4 as described in Equation 2.6;
  Modify the type C (except l_4 and r_4) and the type E control points to achieve C^1 continuity across the interior boundaries;
until *repeated specific number of times*;
Update the values of l_4 and r_4 as described in Equation 2.3;
Modify the type C (except l_4 and r_4) and the type E control points to achieve C^1 continuity across the interior boundaries;

Algorithm 1: Improved Clough-Tocher Interpolant

Figure 2.5 shows the difference between the cubic surfaces provided by the cubic precision and Kashyap's Clough-Tocher algorithms. The loop in Algorithm 1 was repeated 10 times for these results. As can be seen, the surface provided by Kashyap's scheme has an obvious improvement.

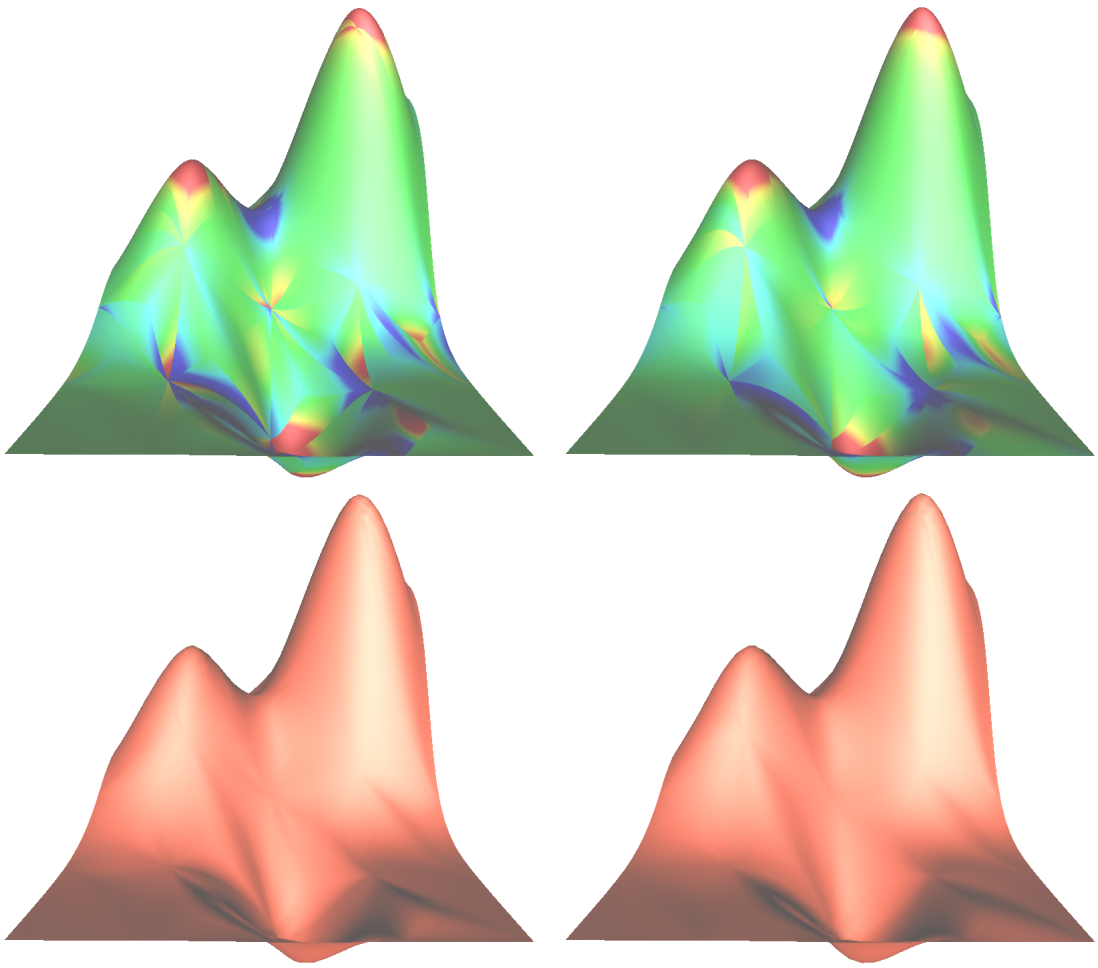

Figure 2.5: The difference between the cubic surfaces provided by the cubic precision (left) and Kashyap's (right) Clough-Tocher algorithms

Chapter 3

Quartic Clough-Tocher Interpolants

In this section I will modify the basic Clough-Tocher scheme to obtain a better surface. The degree of the interpolant is increased from cubic to quartic. The layout of control points is shown in Figure 3.1 and 3.2. For convenience, I classify these control points into five categories:

Type A:	$P_1, P_2, l_6, l_9, r_6, r_9, c_1, c_3$ in Figure 3.1,
	$P, Q, R, p_1, p_2, p_6, q_1, q_2, q_6, r_1, r_2, r_6$ in Figure 3.2.
Type B:	c_2 in Figure 3.1,
	p_3, q_3, r_3 in Figure 3.2.
Type C:	$l_3, l_5, l_7, l_8, r_3, r_5, r_7, r_8$ in Figure 3.1,
	$p_4, p_5, p_7, q_4, q_5, q_7, r_4, r_5, r_7$ in Figure 3.2.
Type D:	$l_1, l_2, l_4, r_1, r_2, r_4$ in Figure 3.1,
	$p_8, p_9, q_8, q_9, r_8, r_9$ in Figure 3.2.
Type E:	S in Figure 3.1,
	S in Figure 3.2.

Type A points are determined by the positions and the first partial derivatives of the vertices, so they will be treated as constants in this thesis.

Type B points lie on the exterior boundaries. Cubic exterior boundaries have no type B control points. For quartics, type B control points are the control points on the exterior boundaries that can be modified, while allowing the patch to still interpolate the positions and normals at the corners.

Type C and D points lie inside the mini-triangles, and on the interior boundaries. Some of them are set to achieve C^1 continuity. The difference between type C and D is that the

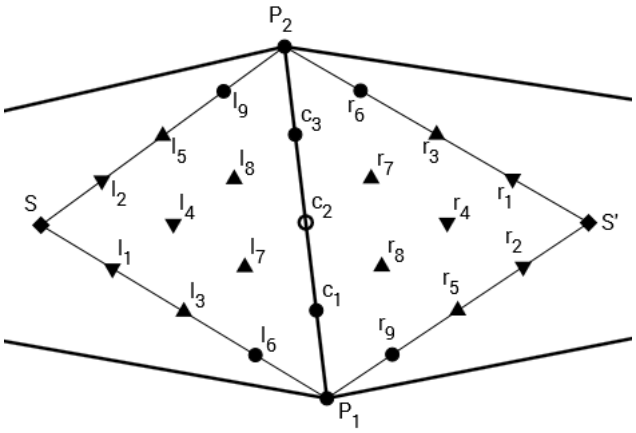

Figure 3.1: An exterior boundary across macro-triangles

- • Type A control points.
- ○ Type B control points.
- ▲ Type C control points.
- ▼ Type D control points.
- ♦ Type E control points.

values of type C points are independent from the values of the type D points, while the values of the type D points are based on the values of the type C points.

Type E points must be coplanar with the surrounding type D points to achieve C^1 continuity.

The approach used in this thesis is to use quartic control points obtained by degree raising the cubic precision surface described in Section 2.1.

3.1 Exterior Fairing with Cubic Exterior Boundary

I begin with the exterior fairing across the exterior boundaries. In Figure 3.1, let (u, v, w) be the barycentric coordinates of S' with respect to $\triangle SP_1P_2$, and let (u', v', w') be the barycentric coordinates of S with respect to $\triangle S'P_2P_1$. In this section I fix the the exterior boundary, which means the z-value of the type A and B points are set by the positions and the tangents of vertices. Now consider the type C points: the z-values of l_7 and r_8

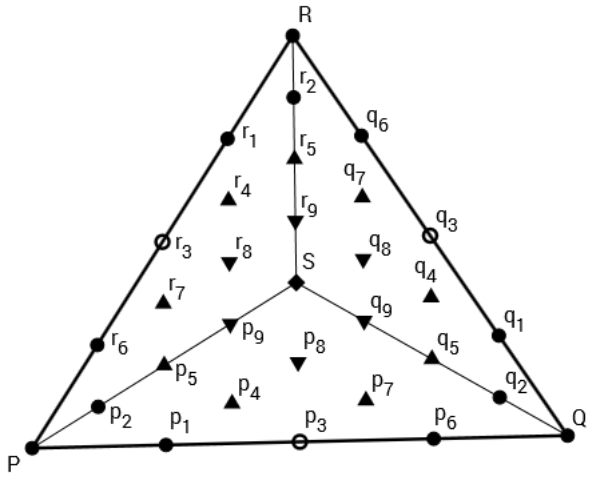

Figure 3.2: Interior boundaries inside a macro-triangle

- • Type A control points.
- ○ Type B control points.
- ▲ Type C control points.
- ▼ Type D control points.
- ♦ Type E control points.

need to satisfy the conditions

$$\begin{array}{rcl} ul_7 + vc_1 + wc_2 & = & r_8 \\ ul_3 + vl_6 + wl_7 & = & u'r_5 + v'r_8 + w'r_9 \end{array} \tag{3.1}$$

to meet the C^1 and C^2 continuity conditions across the exterior boundary. Since c_1, c_2, l_3, l_6, r_5, and r_9 are known, the values of l_7 and r_8 are unique. A similar analysis applies to the values of l_8 and r_7:

$$\begin{array}{rcl} ul_8 + vc_2 + wc_3 & = & r_7 \\ ul_5 + vl_8 + wl_9 & = & u'r_3 + v'r_6 + w'r_7. \end{array} \tag{3.2}$$

Solving (3.1) for l_7 and r_8 and (3.2) for l_8 and r_7 gives

$$\begin{array}{rcl} l_7 & = & (s_1 + t_1)/2uw \\ l_8 & = & (s_2 + t_2)/2uv \\ r_7 & = & (s_2 - t_2)/2v \\ r_8 & = & (s_1 - t_1)/2w, \end{array} \tag{3.3}$$

where

$$\begin{array}{rcl} s_1 & = & -u^2 l_3 - uvl_6 + r_5 - vr_9 \\ s_2 & = & -u^2 l_5 - uwl_9 + r_3 - wr_6 \\ t_1 & = & -vwc_1 - w^2 c_2 \\ t_2 & = & -v^2 c_2 - vwc_3. \end{array}$$

With the values of l_7, l_8, r_7, and r_8 in (3.3), two of the three C^2 continuity conditions described in (1.2) are satisfied. Now consider the type D points. The C^2 condition across the macro-boundary leaves a degree of freedom for the values of l_4 and r_4. This degree of freedom may be used to smooth the surface by minimizing the C^3 discontinuity across the exterior boundary as follows. As shown in Figure 1.4, if c_1' and c_3' are the extension points of $\triangle l_3 l_6 l_7$ and $\triangle l_5 l_8 l_9$, then

$$\begin{array}{rcl} c_1' & = & ul_3 + vl_6 + wl_7 \\ c_3' & = & ul_5 + vl_8 + wl_9. \end{array}$$

To meet with C^2 continuity, these points are also the extension points of $\triangle r_5 r_8 r_9$ and $\triangle r_3 r_6 r_7$. Substituting the values of l_7 and l_8 from (3.3) gives

$$\begin{array}{rcl} c_1' & = & (u^2 l_3 + uvl_6 + r_5 - vr_9 + t_1)/2u \\ c_3' & = & (u^2 l_5 + uwl_9 + r_3 - wr_6 + t_2)/2u. \end{array}$$

Then the C^3 discontinuity can be minimized using least squares by taking the sum of the squares of the differences between each side of Equations (1.3),

$$\begin{array}{l}((u(ul_2+vl_4+wl_5)+vc_2'+wc_3')-(u'r_1+v'r_3+w'r_4))^2\\ \quad +((u(ul_1+vl_3+wl_4)+vc_1'+wc_2')-(u'r_2+v'r_4+w'r_5))^2,\end{array} \tag{3.4}$$

with the constraint that the extension points of $\triangle l_4 l_7 l_8$ and $\triangle r_4 r_7 r_8$ must be equal:

$$ul_4+vl_7+wl_8=u'r_4+v'r_7+w'r_8. \tag{3.5}$$

Recall that c_2' is the extension point of $\triangle l_4 l_7 l_8$ and $\triangle r_4 r_7 r_8$. Then Equation (3.5) can be rewritten as

$$\begin{array}{rcl} l_4 & = & u'c_2'+v'l_8+w'l_7 \\ r_4 & = & uc_2'+vr_8+wr_7. \end{array} \tag{3.6}$$

Substituting these values of l_4 and r_4 into (3.4), the C^3 discontinuity can be rewritten as

$$(e_1+f_1c_2')^2+(e_2+f_2c_2')^2 \tag{3.7}$$

where

$$\begin{array}{rcl} e_1 & = & u^2l_2+uwl_5+uvw'l_7+uvv'l_8-u'r_1-v'r_3-ww'r_7-vw'r_8+wa_2 \\ e_2 & = & u^2l_1+uvl_3+uww'l_7+uwv'l_8-u'r_2-w'r_5-wv'r_7-vv'r_8+va_1 \\ f_1 & = & 3v \\ f_2 & = & 3w. \end{array}$$

Taking the derivative of (3.7), and setting it to zero, gives the value of the extension point c_2' that minimizes the C^3 discontinuity:

$$c_2'=-(e_1f_1+e_2f_2)/(f_1^2+f_2^2). \tag{3.8}$$

The values of l_4 and r_4 can now be calculated by Equation (3.6). After this step, the patches will meet with C^2 continuity with a minimal C^3 discontinuity across the exterior boundaries.

3.2 Interior Fairing

In this section, I give a scheme to smooth the surface inside each macro-triangle. Kashyap's method for the cubic case will be modified and applied here. For the quartic case, order three continuity can be achieved, so one more step is required.

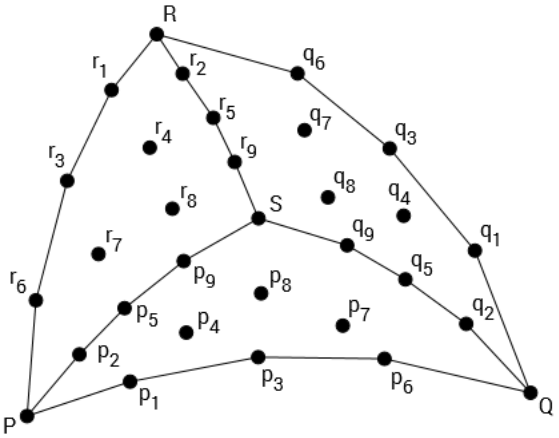

Figure 3.3: 3-D view of continuity conditions of a split macro-triangle: the layout of control points

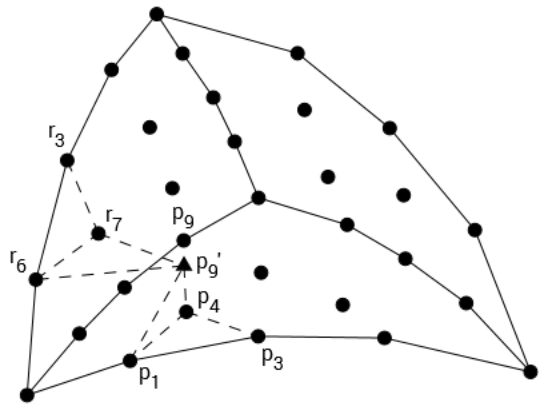

Figure 3.4: 3-D view of continuity conditions of a split macro-triangle: the first C^2 continuity condition

Since S is the center of $\triangle PQR$ on the xy-plane, $S = (P+Q+R)/3$, and thus $Q = -R-P+3S$ and $R = -P-Q+3S$. So the barycentric coordinates of Q with respect to $\triangle RPS$ and the barycentric coordinates of R with respect to $\triangle PQS$ are $(-1,-1,3)$. Thus to achieve C^2 continuity across the interior boundary PS, according to the conditions of C^2 continuity (1.2), the conditions

$$\begin{array}{rcll} -r_3 - r_6 + 3r_7 & = & -p_1 - p_3 + 3p_4 & (a) \\ -r_4 - r_7 + 3r_8 & = & -p_4 - p_7 + 3p_8 & (b) \\ -r_5 - r_8 + 3r_9 & = & -p_8 - q_7 + 3q_9 & (c) \end{array} \tag{3.9}$$

must be satisfied. Notice that Equation (3.9) (c) is always satisfied since both sides are equal to q_8 by the C^1 continuity conditions. Furthermore, if similar analyses are applied to other two interior boundaries, the three extension points (b) of (3.9) for all three interior boundaries are all the same. Thus the conditions of interior C^2 continuity can be written as

$$\begin{array}{rcl} p'_9 & = & 3r_7 - r_3 - r_6 \\ & = & 3p_4 - p_1 - p_3 \\ q'_9 & = & 3p_7 - p_3 - p_6 \\ & = & 3q_4 - q_1 - q_3 \\ r'_9 & = & 3q_7 - q_3 - q_6 \\ & = & 3r_4 - r_1 - r_3 \\ S' & = & 3p_8 - p_4 - p_7 \\ & = & 3q_8 - q_4 - q_7 \\ & = & 3r_8 - r_4 - r_7, \end{array} \tag{3.10}$$

as shown in Figure 3.4 and Figure 3.5. The values of p'_9, q'_9, and r'_9 in the first six lines are deduced from (a), and the value of S' in the rest lines are deduced from (b) in Equation (3.9).

For C^3 continuity across the interior boundary PS, according to the conditions of C^3 continuity (1.3), the conditions

$$\begin{array}{rcl} -r'_9 - p'_9 + 3S' & = & q'_9 \\ -S' - p_4 + 3p_8 & = & p_7 \end{array}$$

must be satisfied. The second equation is satisfied by the conditions of C^2 continuity. Furthermore, for all interior boundaries, the C^3 continuity condition is that all four extension points must be coplanar, i.e.,

$$3S' = p'_9 + q'_9 + r'_9, \tag{3.11}$$

as shown in Figure 3.6.

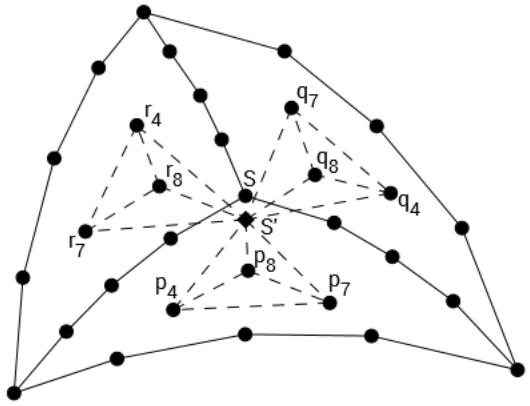

Figure 3.5: 3-D view of continuity conditions of a split macro-triangle: the second C^2 continuity condition

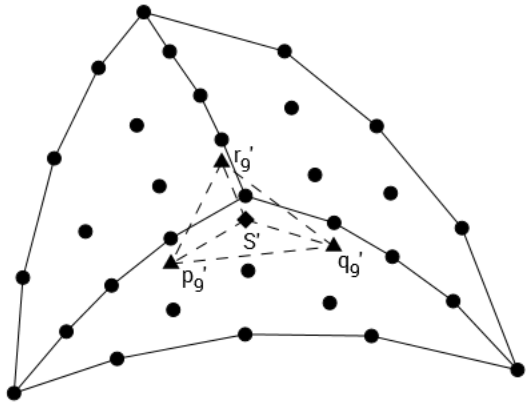

Figure 3.6: 3-D view of continuity conditions of a split macro-triangle: the C^3 continuity condition

In this scheme, all these conditions are satisfiable, but the values of p'_9, q'_9, and r'_9 are not unique. I used least squares forms to obtain the values that minimize the movement of the center control points. Let $\bar{p}$ denote the original value of point p. The value of

$$(p_4 - \bar{p}_4)^2 + (r_7 - \bar{r}_7)^2$$

is minimized, subject to the C^2 continuity constraints

$$3r_7 - r_3 - r_6 = 3p_4 - p_1 - p_3,$$

to find the values of p_4 and r_7 then p'_9 by (3.10). Similar analyses can be applied to the other two corners. The solution to the constrained least squares problem is

$$\begin{array}{rcl} p'_9 & = & 3(\bar{p}_4 + \bar{r}_7)/2 - (p_1 + p_3 + r_3 + r_6)/2 \\ q'_9 & = & 3(\bar{q}_4 + \bar{p}_7)/2 - (q_1 + q_3 + p_3 + p_6)/2 \\ r'_9 & = & 3(\bar{r}_4 + \bar{q}_7)/2 - (r_1 + r_3 + q_3 + q_6)/2 \\ p_4 & = & 3p'_9 - p_1 - p_3 \\ p_7 & = & 3q'_9 - p_3 - p_6 \\ q_4 & = & 3q'_9 - q_1 - q_3 \\ q_7 & = & 3r'_9 - q_3 - q_6 \\ r_4 & = & 3r'_9 - r_1 - r_3 \\ r_7 & = & 3p'_9 - r_3 - r_6. \end{array} \tag{3.12}$$

The values of S', p_8, q_8, and r_8 can be obtained from Equation (3.10) and (3.11):

$$\begin{array}{rcl} S' & = & (p'_9 + q'_9 + r'_9)/3 \\ p_8 & = & (p_4 + p_7 + S')/3 \\ q_8 & = & (q_4 + q_7 + S')/3 \\ r_8 & = & (r_4 + r_7 + S')/3. \end{array} \tag{3.13}$$

Algorithm 2 shows the process of the quartic Clough-Tocher interpolant.

Figure 3.7 shows the difference between the cubic surface provided by Kashyap's Clough-Tocher algorithm and the surface provided by the quartic Clough-Tocher algorithm. The loop in Algorithm 2 was repeated 10 times for these results. The order of the surface is increased from three to four. However, while there is some improvement in the curvature plot, the shaded images are similar and any improvement is not obvious. Additional modification is necessary to improve the surface quality.

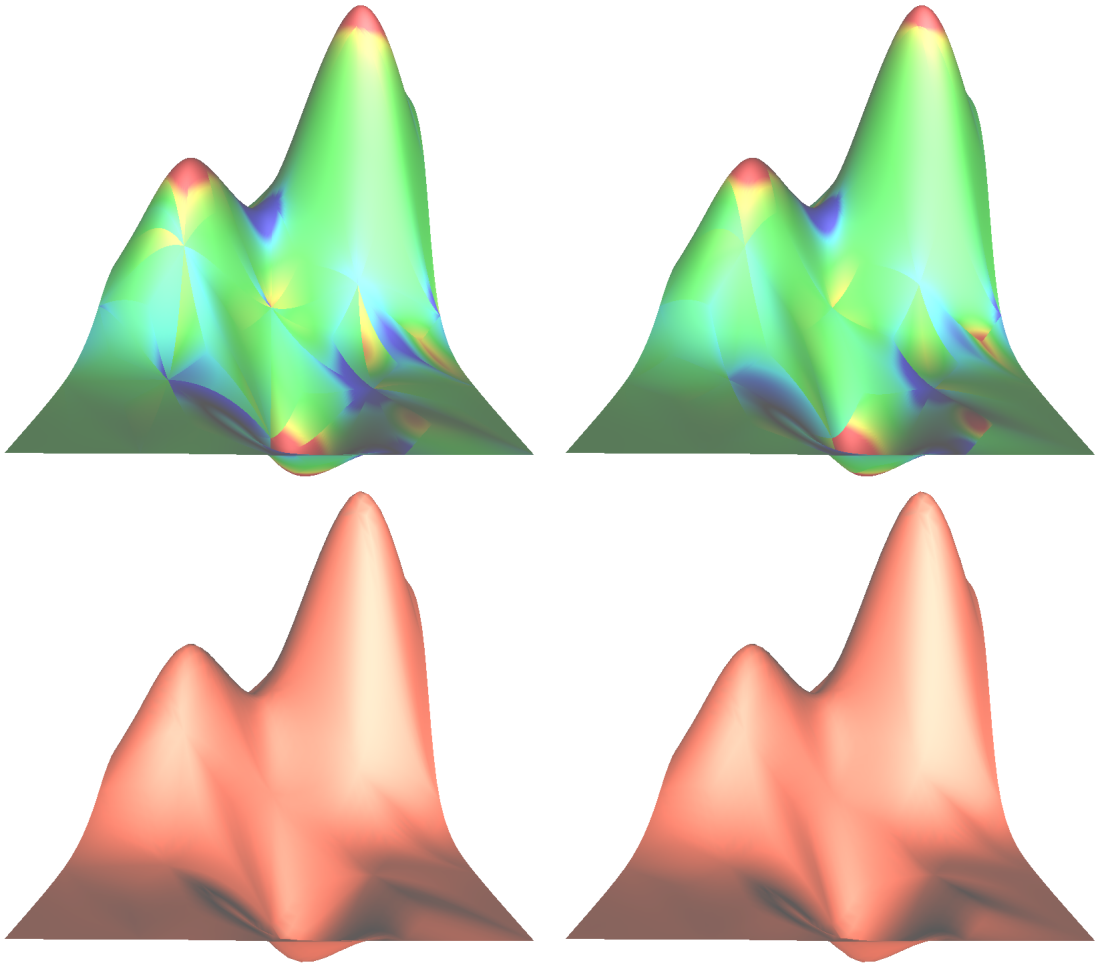

Figure 3.7: The difference between the cubic surface provided by Kashyap's (left) Clough-Tocher algorithm and the quartic surface provided by quartic (right) Clough-Tocher algorithm

Set the control points values to have cubic precision as described in Section 2.1;
Obtain the initial values of the quartic control points by degree raising;
// **Quartic fairing steps repeat**
  Update the values of the center control points l_4, l_7, l_8, r_4, r_7, and r_8 as described in Equation (3.3) and (3.6);
  Update the values of the center control points p_4, p_7, p_8, q_4, q_7, q_8, r_4, r_7, and r_8 as described in Equation (3.12) and (3.13);
  Modify the type C, D, and E control points (except the center control points) to achieve C^1 continuity across the interior boundaries;
until *repeated specific number of times*;
Update the values of the center control points l_4, l_7, l_8, r_4, r_7, and r_8 as described in Equation (3.3) and (3.6);
Modify the type C, D, and E control points (except the center control points) to achieve C^1 continuity across the interior boundaries;

Algorithm 2: Quartic Clough-Tocher Interpolant: Fixed Exterior Boundaries

3.3 Exterior Fairing with Modified exterior boundary

As a second attempt to improve the shape of the quartic Clough-Tocher surface, I will adjust the boundary center points. In particular, I will adjust the value of c_2 in Figure 3.1 to achieve better shape. When using Equation (3.8), for a given value of c_2, there exists a corresponding c_2' and a C^3 discontinuity value across the exterior boundary. The first idea is to treat c_2 as a variable, and minimize the C^3 discontinuity value across the exterior boundary. However, if the value of c_2' (3.8) obtained in Section 3.1

$$c_2' = -(e_1 f_1 + e_2 f_2)/(f_1^2 + f_2^2)$$

is substituted into the formula for C^3 discontinuity (3.7)

$$(e_1 + f_1 c_2')^2 + (e_2 + f_2 c_2')^2,$$

the result will be

$$\begin{aligned}
&(e_1 + f_1 c_2')^2 + (e_2 + f_2 c_2')^2 \\
&= (e_1 - f_1 \frac{e_1 f_1 + e_2 f_2}{f_1^2 + f_2^2})^2 + (e_2 - f_2 \frac{e_1 f_1 + e_2 f_2}{f_1^2 + f_2^2})^2 \\
&= (\frac{e_1 f_2^2 - e_2 f_1 f_2}{f_1^2 + f_2^2})^2 + (\frac{e_2 f_1^2 - e_1 f_1 f_2}{f_1^2 + f_2^2})^2 \\
&= \frac{(e_1 f_2 - e_2 f_1)^2}{(f_1^2 + f_2^2)}.
\end{aligned}$$

e_1 and e_2 can be rewritten as

$$\begin{aligned} e_1 &= p_1 + q_1 c_2 \\ e_2 &= p_2 + q_2 c_2, \end{aligned}$$

where

$$\begin{aligned} p_1 &= u^2 l_2 + \frac{3}{2} uw l_5 + \frac{1}{2} w^2 l_9 - u' r_1 - \frac{3}{2} v' r_3 + \frac{1}{2} w v' r_6 - v^2 w' c_1 - \frac{1}{2} w^2 w' c_3 \\ p_2 &= u^2 l_1 + \frac{3}{2} uv l_3 + \frac{1}{2} v^2 l_6 - u' r_2 - \frac{3}{2} w' r_5 + \frac{1}{2} v w' r_9 - \frac{1}{2} v^2 v' c_1 - w^2 v' c_3 \\ q_1 &= -\frac{3}{2} v^2 v' \\ q_2 &= -\frac{3}{2} w^2 w'. \end{aligned}$$

Thus

$$\begin{aligned} & e_1 f_2 - e_2 f_1 \\ &= (p_1 + q_1 c_2) f_2 - (p_2 + q_2 c_2) f_1 \\ &= (p_1 f_2 - p_2 f_1) + (q_1 f_2 - q_2 f_1) c_2 \\ &= (p_1 f_2 - p_2 f_1) - \frac{9}{2} (v^2 w v' - v w^2 w') c_2 \\ &= (p_1 f_2 - p_2 f_1), \end{aligned}$$

which is a constant. Thus it is impossible to modify c_2 by minimizing the C^3 discontinuity. Instead, the previous approach will be modified to provide another relationship between the value of c_2 and some other control points. In particular the movement of l_4 and r_4

$$(u' c_2' + v' l_8 + w' l_7 - \bar{l}_4)^2 + (u c_2' + v r_8 + w r_7 - \bar{r}_4)^2$$

will be minimized, similar to what was done in Section 3.2. Let $\bar{l}_4$ and $\bar{r}_4$ be the original value of points l_4 and r_4. The value of c_2' that minimizes the movement of l_4 and r_4 is

$$c_2' = (u' \bar{l}_4 + u \bar{r}_4 - \frac{v'}{2v}(s_2 + t_2) - \frac{w'}{2w}(s_1 + t_1) - \frac{uv}{2w}(s_1 - t_1) - \frac{uw}{2v}(s_2 - t_2))/(u^2 + u'^2),$$

which can be rewritten as

$$c_2' = m + n c_2,$$

where

$$\begin{aligned} m &= (u' \bar{l}_4 + u \bar{r}_4 - \frac{u'w' + u^2 v}{2uw} s_1 - \frac{u'v' + u^2 w}{2uv} s_2 \\ &\quad - \frac{uv^2 + u'w'^2}{2} c_1 - \frac{uw^2 + u'v'^2}{2} c_3)/(u^2 + u'^2) \\ n &= -(uvw + u'v'w')/(u^2 + u'^2). \end{aligned}$$

Substituting this new value of c_2' into (3.7) and minimizing, the value of c_2 is

$$c_2 = -\frac{(p_1 + f_1 m)(q_1 + f_1 n) + (p_2 + f_2 m)(q_2 + f_2 n)}{(q_1 + f_1 n)^2 + (q_2 + f_2 n)^2}.$$

Now we have a new value of c_2 that can used in the method in Section 3.1 and 3.2 to calculate the values of the rest of the control points.

Notice that this scheme is used only for finding a new value for c_2, and the movement minimizing process is not used to adjust l_4 and r_4. After getting this new value of c_2, the previous exterior scheme in Section 3.1 will be applied. Algorithm 3 shows the process of quartic Clough-Tocher interpolant with boundary modification.

Set the control point values to have cubic precision as described in Section 2.1;
Obtain the initial values of the quartic control points by degree raising;
// **Quartic fairing steps repeat**
  Update the values of the center control points l_4, l_7, l_8, r_4, r_7, and r_8 as described in Equation (3.3) and (3.6);
  Update the values of the center control points p_4, p_7, p_8, q_4, q_7, q_8, r_4, r_7, and r_8 as described in Equation (3.12) and (3.13);
  Modify the type C, D, and E control points (except the center control points) to achieve C^1 continuity across the interior boundaries;
until *repeated specific number of times*;
// **Boundary modification steps repeat**
  Update the values of c_2 as described in Section 3.3;
  Update the values of the center control points l_4, l_7, l_8, r_4, r_7, and r_8 as described in Equation (3.3) and (3.6);
  Modify the type C, D, and E control points (except the center control points) to achieve C^1 continuity across the interior boundaries;
until *repeated specific number of times*;

Algorithm 3: Quartic Clough-Tocher Interpolant: Modified Exterior Boundaries

Figure 3.8 shows the difference between the quartic surfaces provided by quartic Clough-Tocher algorithms without and with boundary modification. The two loops in Algorithm 3 were both repeated 10 times for these results. As can be seen, the modifications of the quartic exterior boundaries provide a significant improvement.

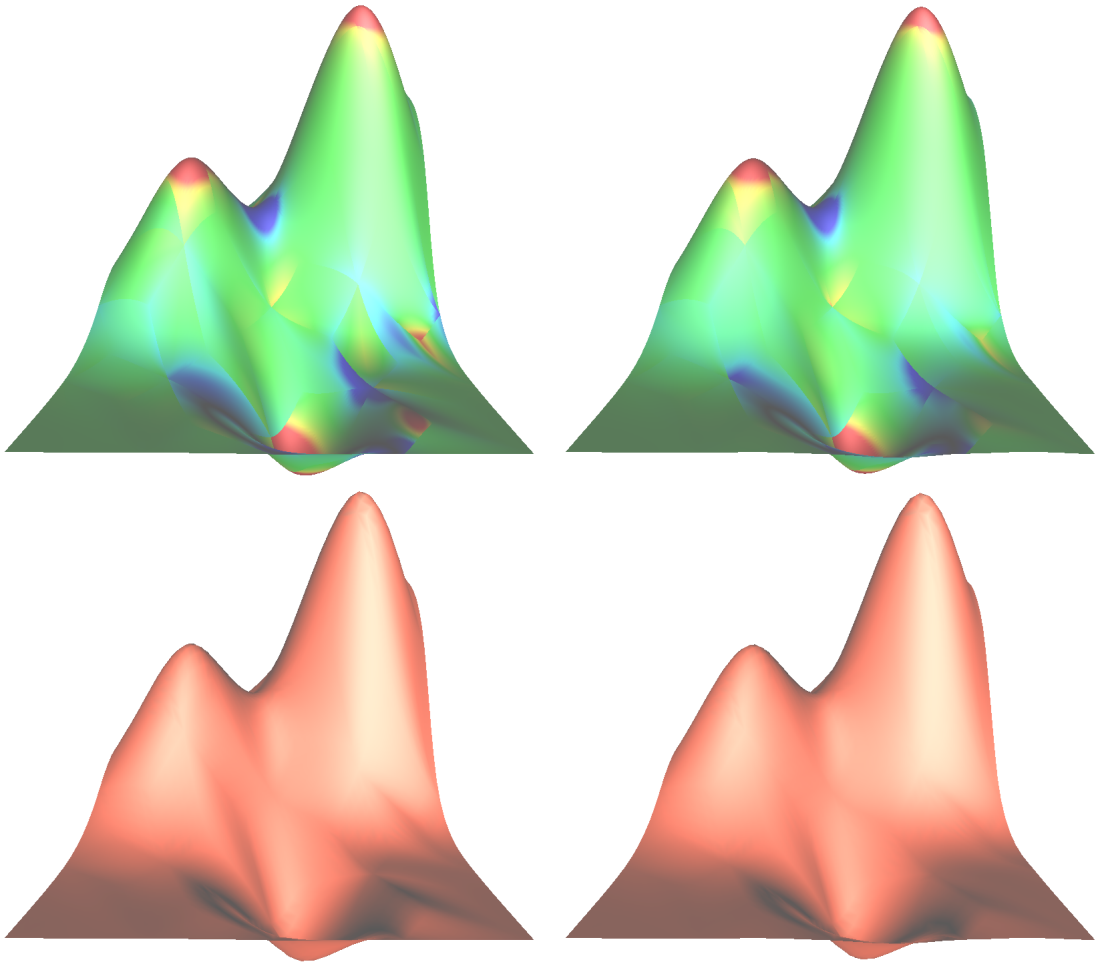

Figure 3.8: The difference between the quartic surfaces provided by quartic Clough-Tocher algorithms without (left) and with (right) boundary modification

Chapter 4

Improvement of the Degree of Continuity

In Chapter 3, I developed a C^1 piecewise quartic polynomial surface with better shape than earlier cubic surfaces. Altough the C^2 continuity conditions are satisfied during the exterior fairing step, the final surface is only C^1 continuous. In this chapter, I will modify the Clough-Tocher algorithms so that the resulting surfaces have the continuity of both the exterior and the interior algorithms, although the interior algorithm will provide only the C^1 smoothness of the original Clough-Tocher algorithm.

4.1 Matrix Representation

In this thesis, the processes of all algorithms contain only linear operations. We can represent the process of the algorithms by matrix operations, and store the values of all control points inside a single column matrix. Then the processes of an algorithm can be described as

$$v \to Mv + t,$$

where M and t are constant. Let $f^{ex}(v) = M_{ex}v + t_{ex}$ denote the exterior fairing process and $f^{in}(v) = M_{in}v + t_{in}$ denote the interior fairing process (with the C^1 smoothing). Then a complete loop can be described as

$$f(v) = M_{in}(M_{ex}v + t_{ex}) + t_{in}. \tag{4.1}$$

If this algorithm converges, with any arbitrary initial value, then the values of the control points will eventually reach a limit v_1:

$$v_1 = M_{in}(M_{ex}v_1 + t_{ex}) + t_{in}.$$

Writing $v_2 = f^{ex}(v_1)$, there exist relationships

$$\begin{array}{rcll} v_1 & = & M_{in}v_2 + t_{in} & (a) \\ v_2 & = & M_{ex}v_1 + t_{ex} & (b). \end{array} \tag{4.2}$$

The surface represented by v_1 is provided by interior fairing and the surface represented by v_2 is provided by exterior fairing. In general the limit of v_1 are not equal to the limit of v_2, and we need to choose one of them as the final result. However consider the following proposition:

Proposition 4.1.1. *Suppose that the repeated application of Equation (4.1) converges, then Equations (4.2) hold. In these equations if the subset of the control points updated by (a) in v_2 and the subset of the control points updated by (b) in v_1 are mutually exclusive, then $v_1 = v_2$.*

Proof. Let n denote the length of v_1 and v_2. Then for any index $i \in \{1, 2, \ldots, n\}$, since the set of the elements updated by (a) in v_2 and the set of the elements updated by (b) in v_1 are mutually exclusive, the i-th element cannot be updated in both (a) and (b) at the same time. There exists one step, (a) or (b), in which the i-th element remains the same. Thus we have $v_1[i] = v_2[i]$ for any index $i \in \{1, 2, \ldots, n\}$, and so $v_1 = v_2$. □

This means that if each varying control point is updated in only one fairing step, then $v_1 = v_2$. However, for Algorithm 2 and Algorithm 3, the center control points (l_4 and r_4 in Figure 1.6 for cubic case and l_4, l_7, l_8, r_4, r_7, and r_8 in Figure 3.1 for quartic case) are updated in both exterior and interior fairing processes. So in general these kind of control points have different values in v_1 and v_2. If the iterations of the algorithm are applied an infinite number of times, the resulting surface will switch between two different values.

4.2 Modified Process of Clough-Tocher Interpolant

In this section, we will modify the Clough-Tocher algorithm by reducing the number of loops used in Kashyap's algorithm, and follow that by repeated application of the exterior fairing and a C^1 smoothing process. Since the C^1 smoothing process updates only the

values of control points on the interior boundaries and S by locating them on the plane formed by adjacent control points, there is no overlap between two groups of control points in each step. By Proposition 4.1.1, this means that $v_1 = v_2$ in Equations (4.2), and the final surface will have the continuity properties of both steps.

For the cubic case, the limit surface we obtained will have C^1 continuity everywhere. However, since this surface is directly provided by the exterior fairing process which minimizes C^2 discontinuity, it should have similar or better quality than the original cubic Clough-Tocher surface. Algorithm 4 shows the process of modified Clough-Tocher interpolant.

Set the type A control points by the locations and derivatives of vertices to achieve C^1 continuity around vertices;
Set the type C control points by the cubic precision Clough-Tocher scheme described in Section 2.1;
Set the type E control points to achieve C^1 continuity across the interior boundaries;
// **Kashyap's fairing steps repeat**
  Update the values of l_4 and r_4 as described in Equation 2.3;
  Update the values of p_4, q_4 and r_4 as described in Equation 2.6;
  Modify the type C (except l_4 and r_4) and the type E control points to achieve C^1 continuity across the interior boundaries;
until *repeated specific number of times*;
// **Exterior fairing and C^1 smoothing repeat**
  Update the values of l_4 and r_4 as described in Equation 2.3;
  Modify the type C (except l_4 and r_4) and the type E control points to achieve C^1 continuity across the interior boundaries;
until *repeated specific number of times*;

Algorithm 4: Modified Kashyap's Interpolant

Figure 4.1 shows the difference between the cubic surfaces provided by Kashyap's and the modified Clough-Tocher algorithms. The first loop of Algorithm 4 was repeated twice and the second loop was repeated 8 times for these results. As can be seen, the surfaces have similar qualities, and the modified surface has smaller curvature discontinuity across the exterior boundaries. For example, the boundaries pointed to by red and blue arrows in Figure 4.1 show a lower curvature discontinuity for the new scheme.

For the quartic case, the limit surface we obtained will be C^2 across the macro-boundaries, and C^1 across the interior boundaries. The "partial" C^2 continuity surface exists when the algorithm converges. In my test cases, the algorithm always converged.

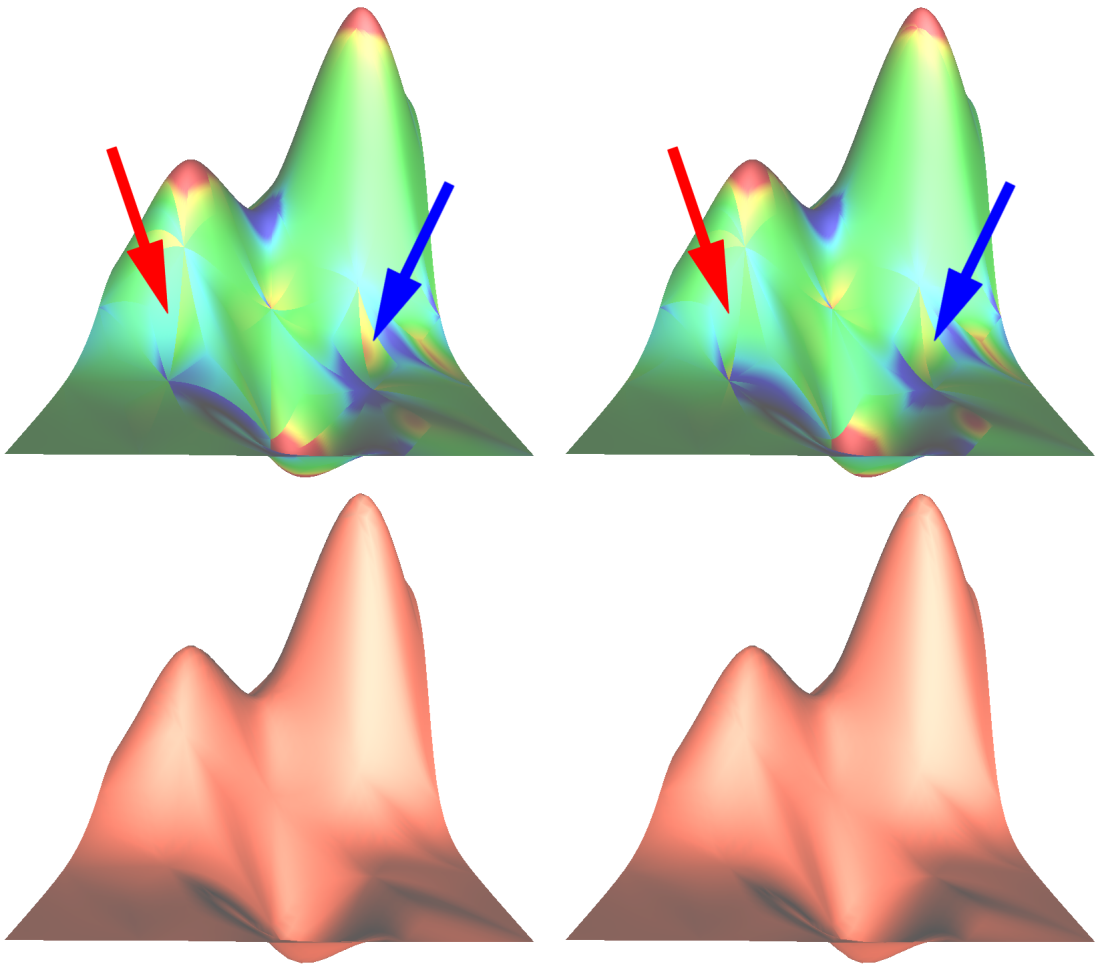

Figure 4.1: The difference between the cubic surfaces provided by Kashyap's (left) and the modified (right) Clough-Tocher algorithms

Algorithm 5 shows the process of modified quartic Clough-Tocher interpolant. First use the original quartic Clough-Tocher interpolant, followed by the boundary modification, and then follow that by repeated application of the exterior fairing and a C^1 smoothing process. In the following section, I will provide a proof of convergence for restricted input.

Set the control points values to have cubic precision as described in Section 2.1;
Obtain the initial values of the quartic control points by degree raising;
// **Quartic fairing steps repeat**
  Update the values of the center control points l_4, l_7, l_8, r_4, r_7, and r_8 as described in Equation (3.3) and (3.6);
  Update the values of the center control points p_4, p_7, p_8, q_4, q_7, q_8, r_4, r_7, and r_8 as described in Equation (3.12) and (3.13);
  Modify the type C, D, and E control points (except the center control points) to achieve C^1 continuity across the interior boundaries;
until *repeated specific number of times*;
// **Boundary modification steps repeat**
  Update the values of c_2 as described in Section 3.3;
  Update the values of the center control points l_4, l_7, l_8, r_4, r_7, and r_8 as described in Equation (3.3) and (3.6);
  Modify the type C, D, and E control points (except the center control points) to achieve C^1 continuity across the interior boundaries;
until *repeated specific number of times*;
// **Exterior fairing and C^1 smoothing repeat**
  Update the values of the center control points l_4, l_7, l_8, r_4, r_7, and r_8 as described in Equation (3.3) and (3.6);
  Modify the type C, D, and E control points (except the center control points) to achieve C^1 continuity across the interior boundaries;
until *repeated specific number of times*;

Algorithm 5: Modified Quartic Clough-Tocher Interpolant

Figure 4.2 shows the difference between the quartic surfaces provided by the original and the modified Clough-Tocher algorithms with boundary modification. The first loop of the algorithm repeats 2 times, the second repeats 10 times, and the third repeats 8 times for the surface constructed in this figure. As can be seen, the two surfaces have similar quality. However, the original quartic scheme has a C^2 discontinuity of 1.7×10^{-12}, and the modified scheme has a discontinuity of 8.3×10^{-16}. While the C^2 discontinuity of the original quartic scheme is small, it does not decrease after many iterations (for example, the C^2 discontinuity is still 1.7×10^{-12} after 100 iterations in this example).

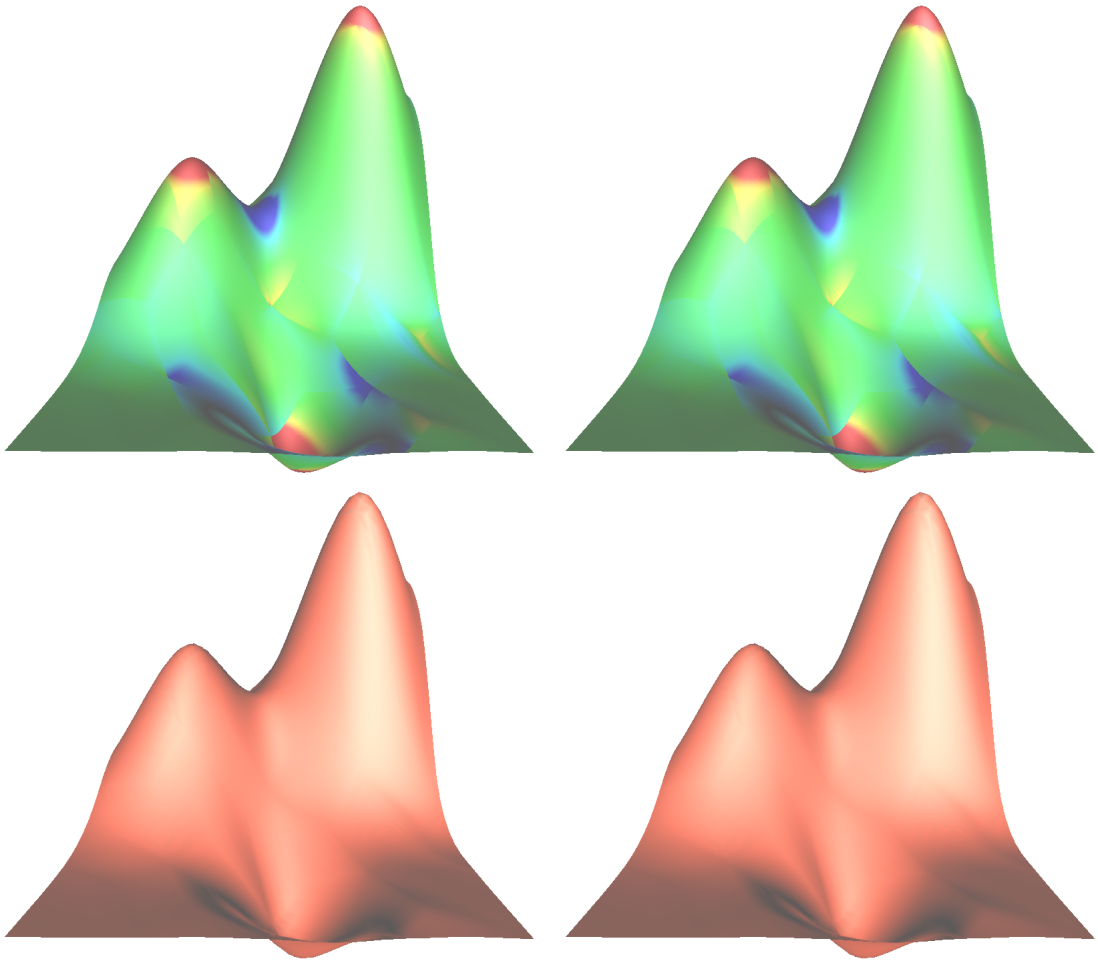

Figure 4.2: The difference between the quartic surfaces provided by the original (left) and the modified (right) Clough-Tocher algorithms with boundary modification

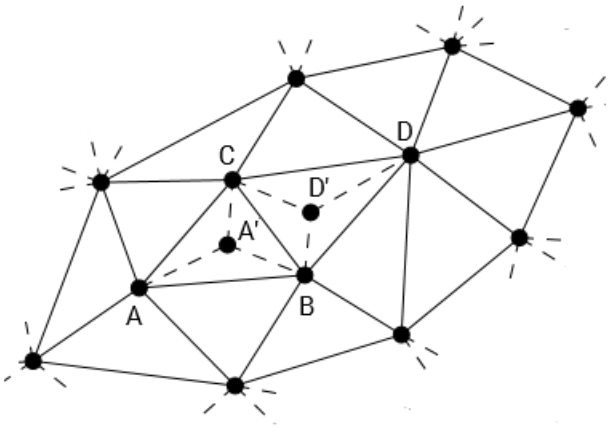

Figure 4.3: An equi-area network

4.3 Convergence of Modified Clough-Tocher Interpolant

In this section, I prove that if the input triangular network satisfies some conditions, then the process described in Section 4.2 will converge to a surface after infinite iterations. The order of continuity across the exterior boundaries of this resulting surface is C^2, and the order of continuity across the other boundaries is C^1.

4.3.1 Equi-Area Network

Definition 4.3.1. *A triangular network N is equi-area if*

1. *N is finite.*
2. *All triangles in N have same area on the xy-plane.*
3. *Any two adjacent triangles in N form a convex quadrilateral.*

For example, the network shown in Figure 4.3 is equi-area. ABC and DCB are two adjacent triangles. If (u, v, w) are the barycentric coordinates of D with respect to $\triangle ABC$, then $u = -1$, $v, w > 0$, and $v + w = 2$. Furthermore, the following proposition can be obtained.

Proposition 4.3.1. *In an equi-area network, if A' and D' are the barycentres of ABC and DCB, and (u', v', w') are the barycentric coordinates of D' with respect to $\triangle A'BC$, then $u' = -1$ and*

$$\frac{2}{3} < v', w' < \frac{4}{3}.$$

Proof. Since the area of ABC is equal to the area of DCB, then the area of $A'BC$ is equal to the area of $D'CB$, thus $u' = -1$. Also since A' and D' are the barycentre of ABC and DCB, then

$$\begin{aligned} v' &= (2v + w)/3 \\ w' &= (v + 2w)/3, \end{aligned}$$

thus since $v + w = 2$,

$$\frac{2}{3} = (v + w)/3 < v', w' < 2(v + w)/3 = \frac{4}{3}.$$

□

In this chapter, we assume that all networks are equi-area.

4.3.2 Cauchy Amplitude

In the iteration schemes, each control point x of the surface can be treated as a sequence $x = \{x_i\}_{i\in\mathbb{N}}$, where x_i is the value of x after i iterations. If all these sequences converge, then the surface converges. To prove convergence, I make the following definition:

Definition 4.3.2. *For any sequence $x = \{x_i\}_{i\in\mathbb{N}}$, its Cauchy amplitude is*

$$k(x) = \sup\{\epsilon \geq 0\text{: } \forall N \in \mathbb{N}^+, \exists m, n > N, \text{ such that } |x_m - x_n| \geq \epsilon\}. \tag{4.3}$$

The Cauchy amplitude is non-negative. If a real number sequence has a zero Cauchy amplitude, then it is a Cauchy sequence, and converges.

Proposition 4.3.2. *For any sequences $x = \{x_i\}_{i\in\mathbb{N}}$, $y = \{y_i\}_{i\in\mathbb{N}}$ and $N \in \mathbb{N}^+$ that satisfy $x_{i+t} = y_i$ for any $i \geq N$ and some fixed $t \in \mathbb{N}$,*

$$k(x) = k(y).$$

Proof. The proposition follows directly from the definition of Cauchy amplitude (4.3). □

Proposition 4.3.3. *For any sequence $x = \{x_i\}_{i\in\mathbb{N}}$ and arbitrary $t_1, t_2 \in \mathbb{R}$,*

$$k(\{t_1 x_i + t_2\}_{i\in\mathbb{N}}) = |t_1| k(x).$$

Proof. By the definition (4.3), we have

$$\forall \epsilon > 0,\ \exists N \in \mathbb{N}^+, \text{ such that } \forall m, n > N,\ |x_m - x_n| < k(x) + \epsilon,$$

where

$$\begin{aligned} & |(t_1 x_m + t_2) - (t_1 x_n + t_2)| \\ = \ & |t_1||x_m - x_n| \\ < \ & |t_1| k(x) + |t_1|\epsilon, \end{aligned}$$

thus

$$k(\{t_1 x_i + t_2\}_{i \in \mathbb{N}}) \leq |t_1| k(x).$$

Also by the definition of k, have

$$\forall N \in \mathbb{N}^+,\ \exists m, n > N, \text{ such that } |x_m - x_n| \geq k(x),$$

where

$$\begin{aligned} & |(t_1 x_m + t_2) - (t_1 x_n + t_2)| \\ = \ & |t_1||x_m - x_n| \\ \geq \ & |t_1| k(x), \end{aligned}$$

thus

$$k(\{t_1 x_i + t_2\}_{i \in \mathbb{N}}) \geq |t_1| k(x).$$

□

Proposition 4.3.4. *For any sequences $x = \{x_i\}_{i \in \mathbb{N}}$, $y = \{y_i\}_{i \in \mathbb{N}}$ and arbitrary $t_1, t_2, t_3 \in \mathbb{R}$,*

$$k(\{t_1 x_i + t_2 y_i + t_3\}_{i \in \mathbb{N}}) \leq |t_1| k(x) + |t_2| k(y).$$

Proof. By the definition (4.3), we have

$$\forall \epsilon > 0,\ \exists N \in \mathbb{N}^+, \text{ such that } \forall m, n > N,\ |x_m - x_n| < k(x) + \epsilon \text{ and } |y_m - y_n| < k(y) + \epsilon,$$

where

$$\begin{aligned} & |(t_1 x_m + t_2 y_m + t_3) - (t_1 x_n + t_2 y_n + t_3)| \\ = \ & |(t_1(x_m - x_n) + t_2(y_m - y_n)| \\ \leq \ & |t_1||x_m - x_n| + |t_2||y_m - y_n| \\ \leq \ & |t_1| k(x) + |t_2| k(y) + (|t_1| + |t_2|)\epsilon, \end{aligned}$$

thus

$$k(\{t_1 x_i + t_2 y_i + t_3\}_{i \in \mathbb{N}}) \leq |t_1| k(x) + |t_2| k(y).$$

□

4.3.3 Convergence of the Exterior Fairing Algorithm

In this section I will provide a proof of the result of convergence in some restricted cases. Given data sites over an equi-area network, the convergence of the quartic construction described in Section 4.2 can be shown with two steps:

1. Apply the exterior fairing algorithm to the exterior boundaries across the macro-triangles to meet the C^2 continuity condition and minimize the C^3 discontinuity.
2. Modify the values of control points on the interior boundaries to meet C^1 continuity inside each macro-triangle.

I split each representation of the new values of the control points into the varying part and a constant part. For example, according to Equation (3.3), the value of l_7 is

$$l_7 = (-u^2 l_3 - uvl_6 + r_5 - vr_9 - vwc_1 - w^2 c_2)/2uw, \tag{4.4}$$

where $u = -1$ and only l_3 and r_5 are varying control points. Let x_1 denote the constant part of (4.4), then its value is

$$x_1 = (-vl_6 + vr_9 + vwc_1 + w^2 c_2)/2w.$$

The other constant values can be obtained by similar analyses. Then for the exterior step we have

$$\begin{array}{rcl} l_7 & \leftarrow & (l_3 - r_5)/2w + x_1 \\ l_8 & \leftarrow & (l_5 - r_3)/2v + x_2 \\ r_7 & \leftarrow & (r_3 - l_5)/2v + x_3 \\ r_8 & \leftarrow & (r_5 - l_3)/2w + x_4 \\ l_4 & \leftarrow & (wl_1 + vl_2 + vr_1 + wr_2)/(3v^2 + 3w^2) \\ & & -vw(l_3 + l_5 + r_3 + r_5)/(2v^2 + 2w^2) \\ & & +(2vl_7 + 2wl_8 - wr_7 - vr_8)/3 + x_5 \\ r_4 & \leftarrow & (wl_1 + vl_2 + vr_1 + wr_2)/(3v^2 + 3w^2) \\ & & -vw(l_3 + l_5 + r_3 + r_5)/(2v^2 + 2w^2) \\ & & +(2wr_7 + 2vr_8 - vl_7 - wl_8)/3 + x_6. \end{array} \tag{4.5}$$

In the second step the center control points inside the macro-triangles are adjusted to meet the C^1 continuity conditions:

$$\begin{array}{rcl} p_5 & \leftarrow & (p_4 + r_7)/3 + x_7 \\ q_5 & \leftarrow & (q_4 + p_7)/3 + x_8 \\ r_5 & \leftarrow & (r_4 + q_7)/3 + x_9 \\ p_9 & \leftarrow & (p_5 + p_8 + r_8)/3 \\ q_9 & \leftarrow & (q_5 + q_8 + p_8)/3 \\ r_9 & \leftarrow & (r_5 + r_8 + q_8)/3 \\ s & \leftarrow & (p_9 + q_9 + r_9)/3. \end{array} \tag{4.6}$$

where all variables above represent the values of control points that may vary during the process.

The first step (4.5) will make the exterior boundaries C^2 and the interior boundaries C^0, and the second step (4.6) will make the exterior boundaries C^0 and the interior boundaries C^1. Claim: if this process is repeated an infinite number of times, then the surface will converge, and the final surface patches will meet with C^2 continuity along the exterior boundaries and with C^1 continuity along the interior boundaries. To prove this, the following lemmas are needed.

Lemma 4.3.1. *In an equi-area network, across an exterior boundary (Figure 3.1),*

$$k(l_7) = k(r_8).$$

Proof. Since

$$\begin{array}{rcl} l_7 & \leftarrow & (l_3 - r_5)/2w + x_1 \\ r_8 & \leftarrow & (r_5 - l_3)/2w + x_4, \end{array}$$

then

$$\begin{array}{rcl} l_7 & = & -r_8 + x_1 + x_4 \\ r_8 & = & -l_7 + x_1 + x_4, \end{array}$$

then by Proposition 4.3.4

$$\begin{array}{rcl} k(l_7) & \leq & k(r_8) \\ k(r_8) & \leq & k(l_7), \end{array}$$

thus

$$k(l_7) = k(r_8).$$

□

Lemma 4.3.2. *In an equi-area network, across an exterior boundary (Figure 3.1), if* $k(l_3) \leq \frac{2}{3}k(l_7)$*, then*

$$k(r_5) \geq \frac{2}{3}k(r_8).$$

Furthermore, if $k(l_3) > 0$*, then*

$$k(r_5) > \frac{2}{3}k(r_8).$$

Proof. Since

$$l_7 \leftarrow (l_3 - r_5)/2w + x_1,$$

then

$$\frac{4}{3}k(l_7) \leq 2wk(l_7) \leq k(l_3) + k(r_5),$$

thus

$$k(r_5) - \frac{2}{3}k(r_8) = k(r_5) - \frac{2}{3}k(l_7) \geq \frac{2}{3}k(l_7) - k(l_3) \geq 0.$$

If $k(l_3) > 0$, then

$$\frac{4}{3}k(l_7) < 2wk(l_7),$$

thus

$$k(r_5) - \frac{2}{3}k(r_8) > 0.$$

□

Lemma 4.3.3. *In an equi-area network, inside a macro-triangle (Figure 3.2), if* $k(p_7) < \frac{3}{2}k(q_5)$*, then*

$$k(q_4) > \frac{3}{2}k(q_5).$$

Proof. Since

$$q_5 \leftarrow (q_4 + p_7)/3 + x_8,$$

then

$$3k(q_5) \leq k(q_4) + k(p_7),$$

thus

$$k(q_4) - \frac{3}{2}k(q_5) \geq \frac{3}{2}k(q_5) - k(p_7) > 0.$$

□

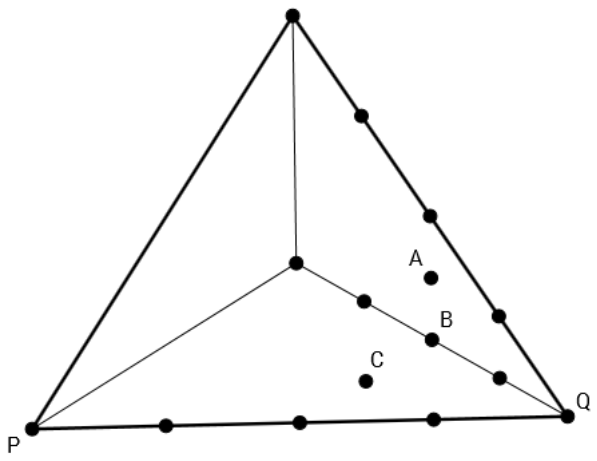

Figure 4.4: A macro-boundary lies on the boundary of the network

Applying these lemmas, the following theorem can be obtained.

Theorem 4.3.1. *In an equi-area network, all varying control points close to the vertices of macro-triangles (l_3, l_7, r_8, and r_5 in Figure 3.1, and p_7, q_5, and q_4 in Figure 3.2) have Cauchy amplitude values of zero.*

Proof. Starting with control points in Figure 3.2, assume by contradiction that $k(q_5) > 0$. Since

$$3k(q_5) \leq k(p_7) + k(q_4),$$

then

$$k(q_5) \leq \frac{2}{3}k(p_7) \text{ or } k(q_5) \leq \frac{2}{3}k(q_4).$$

Applying the above lemmas, a strictly increasing sequence formed by the Cauchy amplitude values of varying control points on the interior boundaries close to a vertex can be formed.

If vertex Q lies on the boundary of the network, then the sequence is finite, and the last element of the sequence is a control point of a macro-triangle adjacent to the network boundary. As shown in Figure 4.4, suppose that PQ is the boundary of the network, and B is the last element of the sequence. Then

$$k(C) = 0 \text{ and } k(B) > \frac{2}{3}k(A) > 0.$$

However, by the propositions of Cauchy amplitude, this means

$$|k(A) - k(C)| \leq 3k(B) \leq k(A) + k(C),$$

and thus

$$k(A) = 3k(B).$$

This contradicts the fact $k(B) > \frac{2}{3}k(A) > 0$. Thus the assumption that $k(q_5) > 0$ is wrong, and so $k(q_5) = 0$ if vertex Q lies on the boundary of the network.

If vertex Q lies inside the network, then the control points around it forms a cycle. Thus the sequence contains a loop. However, the sequence is strictly increasing, which contradicts the fact that the sequence contains a loop. So the assumption that $k(q_5) > 0$ is wrong, thus $k(q_5) = 0$ if vertex Q lies inside the network.

So we always have $k(q_5) = 0$. Similarly, all varying control points close to the vertices of the macro-triangles have Cauchy amplitude values zero. □

Lemma 4.3.4. *In an equi-area network, across an exterior boundary (Figure 3.1),*

$$k(l_4) = k(r_4).$$

Proof. Since

$$\begin{aligned} l_4 \;&\leftarrow\; (wl_1 + vl_2 + vr_1 + wr_2)/(3v^2 + 3w^2) \\ &\quad\; -vw(l_3 + l_5 + r_3 + r_5)/(2v^2 + 2w^2) \\ &\quad\; +(2vl_7 + 2wl_8 - wr_7 - vr_8)/3 + x_5 \\ r_4 \;&\leftarrow\; (wl_1 + vl_2 + vr_1 + wr_2)/(3v^2 + 3w^2) \\ &\quad\; -vw(l_3 + l_5 + r_3 + r_5)/(2v^2 + 2w^2) \\ &\quad\; +(2wr_7 + 2vr_8 - vl_7 - wl_8)/3 + x_6, \end{aligned}$$

then

$$\begin{aligned} l_4 \;&=\; r_4 + vl_7 + wl_8 - wr_7 - vr_8 + x_5 - x_6 \\ r_4 \;&=\; l_4 - vl_7 - wl_8 + wr_7 + vr_8 - x_5 + x_6, \end{aligned}$$

then

$$\begin{aligned} k(l_4) \;&\leq\; k(r_4) \\ k(r_4) \;&\leq\; k(l_4), \end{aligned}$$

thus

$$k(l_4) = k(r_4).$$

□

Lemma 4.3.5. *In an equi-area network, across the exterior boundary (Figure 3.1), if* $k(l_1) + k(l_2) < \frac{4}{3}k(l_4)$, *then*

$$k(r_1) + k(r_2) > \frac{8}{3}k(r_4).$$

Proof. Since

$$\begin{array}{rcl} l_4 & \leftarrow & (wl_1 + vl_2 + vr_1 + wr_2)/(3v^2 + 3w^2) \\ & & -vw(l_3 + l_5 + r_3 + r_5)/(2v^2 + 2w^2) \\ & & +(2vl_7 + 2wl_8 - wr_7 - vr_8)/3 + x_5, \end{array}$$

thus

$$3(v^2 + w^2)k(l_4) \leq wk(l_1) + vk(l_2) + vk(r_1) + wk(r_2).$$

Since

$$v + w = 2 \text{ and } \frac{2}{3} < v, w < \frac{4}{3},$$

then

$$\frac{9}{2}k(l_4) < k(l_1) + k(l_2) + k(r_1) + k(r_2),$$

thus

$$\begin{array}{rcl} & & k(r_1) + k(r_2) - \frac{8}{3}k(r_4) \\ & = & k(r_1) + k(r_2) - \frac{8}{3}k(l_4) \\ & > & \frac{11}{6}k(l_4) - k(l_1) - k(l_2) \\ & > & 0. \end{array}$$

□

Lemma 4.3.6. *In an equi-area network, inside the macro-triangle (Figure 3.2), if* $k(p_9) + k(q_9) > \frac{8}{3}k(p_8)$, *then*

$$k(p_9) + k(r_9) < \frac{4}{3}k(r_8) \text{ or } k(q_9) + k(r_9) < \frac{4}{3}k(q_8).$$

Proof. Since

$$\begin{array}{rcl} p_9 & \leftarrow & (p_5 + p_8 + r_8)/3 \\ q_9 & \leftarrow & (q_5 + q_8 + p_8)/3, \end{array}$$

then

$$2k(p_8) + k(q_8) + k(r_8) \geq 3k(p_9) + 3k(q_9),$$

then

$$2(k(q_8)+k(r_8))-3(k(p_9)+k(q_9)) \geq 3(k(p_9)+k(q_9))-4k(p_8) > 0,$$

thus

$$\begin{aligned}
&(4k(r_8)-3k(p_9)-3k(r_9))+(4k(q_9)-3k(q_9)-3k(r_9)) \\
&= 4k(q_8)+4k(r_8)-3k(p_9)-3k(q_9)-6k(r_9) \\
&= 2(k(q_8)+k(r_8))-3(k(p_9)+k(q_9))+2(k(q_8)+k(r_8)-3k(r_9)) \\
&> 0.
\end{aligned}$$

Thus $k(p_9)+k(r_9) < \frac{4}{3}k(r_8)$ or $k(q_9)+k(r_9) < \frac{4}{3}k(q_8)$. □

Lemma 4.3.7. *In an equi-area network, inside the macro-triangle (Figure 3.2), if* $k(p_9)+k(q_9) > \frac{8}{3}k(p_8)$ *and* $k(p_9)+k(r_9) < \frac{4}{3}k(r_8)$*, then*

$$k(r_8) > k(p_8).$$

Proof. Assume that $k(r_8) \leq k(p_8)$. Since

$$\begin{aligned}
p_9 &\leftarrow (p_5+p_8+r_8)/3 \\
q_9 &\leftarrow (q_5+q_8+p_8)/3,
\end{aligned}$$

then

$$k(p_9) \leq \frac{1}{3}(k(p_8)+k(r_8)) \leq \frac{2}{3}k(p_8),$$

then

$$k(q_9) > \frac{8}{3}k(p_8)-k(p_9) \geq 2k(p_8),$$

thus

$$k(q_8) \geq 3k(q_9)-k(p_8) > 5k(p_8).$$

However

$$k(q_8) \leq 3k(r_9)+k(r_8) \leq 5k(r_8) \leq 5k(p_8).$$

This is a contradiction, so the assumption of $k(r_8) \leq k(p_8)$ is wrong. Thus $k(r_8) > k(p_8)$. □

Applying these lemmas, the following theorem can be obtained.

Theorem 4.3.2. *In an equi-area network, all varying control points close to the center of macro-triangles (*l_1*,* l_2*,* l_4*,* r_1*,* r_2*, and* r_4 *in Figure 3.1, and* p_8*,* p_9*,* q_8*,* q_9*,* r_8*, and* r_9 *in Figure 3.2) have Cauchy amplitude values zero.*

Proof. Starting with control points in Figure 3.2, assume by contradiction that $k(p_8) = 0$ and $k(q_8) > 0$. Then by the above lemmas an increasing sequence

$$S = \{k(a_0), k(b_1), k(a_1), k(b_2), k(a_2), k(b_3), k(a_3), \ldots\}$$

can be obtained, where a_0 is p_8, b_1 is q_8 or r_8, a_i and b_{i+1} are a pair of adjacent center control points inside a macro-triangle, b_i and a_i are pair of center control points across an exterior boundary. The statement $a_i < b_{i+1}$ and $b_i = a_i$ are satisfied.

Since S is an increasing sequence and the network is finite, we know that S is finite, and its last element should be a center control point adjacent to the boundary of the network, which always has a Cauchy amplitude zero. This is a contradiction, so the assumptions that $k(p_8) = 0$ and $k(q_8) > 0$ are wrong, thus the values of $k(p_8)$, $k(q_8)$, and $k(r_8)$ are all zero or all positive.

Since the network is finite, then a macro-triangle that lies on the boundary of the network can always be found, on which exists a center control point adjacent to the boundary of the network. This center control point always has a Cauchy amplitude value zero. Then all three center control points have Cauchy amplitude values zero. By the above lemmas, all varying control points close to the center of macro-triangles have Cauchy amplitude values zero. □

So all control points of the surface have Cauchy amplitude values zero, thus all the sequences will converge. Then we know the restricted algorithm described in Section 4.2 will eventually converge if the input network is equi-area.

Chapter 5

Conclusion

Kashyap's research improved the shape of Clough-Tocher interpolation. This thesis has attempted to improve on Kashyap's results. The following conclusions can be formed from this work.

First, I developed an improved iteration scheme, which constructs a globally C^1 continuous piecewise quartic interpolation surface that has better shape than the cubic ones of Kashyap. This scheme contains two parts. The first part increases the order of Bézier patches used, and applies similar techniques (fairing algorithms) to those used by Kashyap. However, increasing the order only provides limited improvement. The second step is to modify the center control points of the exterior boundaries, which increases the degree of the boundary curves from cubic to quartic. This modification helps eliminate the folds and bumps across the exterior boundaries, and provides a significant shape improvement.

Second, I developed an alternative version of the scheme to provide a specific final limit surface. With the other method, the surface construction alternates between two different values in the limit, and we need to choose one as the final result. I proved that if the algorithm satisfies certain conditions, then a modified process of the algorithm provides a stable result. Furthermore, in the limit, the surface is C^2 continuous across the exterior boundaries of the macro-domain triangle. In addition, I proved that the modified algorithm always converges for some restricted input data.

For future work, as mentioned in Section 4.1, all steps in the algorithms are linear, thus there should exist a method to calculate exact convergent values by solving linear matrix equations. The quartic fairing algorithm has the property that the limits of the control points "close to" data vertices only depend on each single vertex. So part of the fairing

algorithm can be calculated as a matrix equation, and the rest can be solved by same method as applied in the fairing algorithm.

In this thesis, I only tested my schemes on one data set. This data set was chosen as the surface it is based on is a common data set in the field. Further, it is the most difficult of the six Franke functions. schemes that obtain reasonable results on the Franke No.1 data set usually yield excellent results on the other Franke functions, making comparisons difficult (since all schemes do well). However, tests on additional data sets would also be of interest.

Further, the primary quality criteria was visual surface shape. Although somewhat vague and subjective, this metric was chosen over other error metrics since the improvements in shape were readily visible in the resulting surfaces, and it is an important metric in geometric design. Further, other metrics (such as L^2 error metrics, etc.) correspond poorly to visual shape, with lower error values often being given to surfaces with worse shape. While visual quality was sufficient for the work in this thesis, moving forward, additional metrics (shape and otherwise) would also be interesting to explore.

Finally, polynomial surfaces are only one class of interpolatory surfaces. While my work produced some polynomial interpolation schemes that have better shape than some previous polynomial interpolation schemes, a full comparison to non-polynomial schemes would also be of interest.

References

[1] R.W. Clough and J.L. Tocher. Finite element stiffness matrices for analysis of plates in bending. *Proceedings of the Conference on Matrix Methods in Structural Mechanics*, pages 515–545, 1965.

[2] R. Franke. A critical comparison of some methods for interpolation of scattered data, 1979.

[3] P. Kashyap. Improving Clough-Tocher interpolants. *Computer Aided Geometric Design*, 13(7):629–651, 1996.

[4] M. Lai. Geometric interpretation of smoothness conditions of triangular polynomial patches. *Computer Aided Geometric Design*, 14(2):191 – 199, 1997.

[5] M. Lai and L. Schumaker. *Spline Functions on Triangulations*. Number 110. Cambridge University Press, 2007.

[6] S. Mann. Cubic precision Clough-Tocher interpolation. *Computer Aided Geometric Design*, 16(2):85 – 88, 1999.

[7] A. Ženíšek. Interpolation polynomials on the triangle. *Numerische Mathematik*, 15:283–296, 1970.

[8] G. Farin W, Bohm and J. Kahmann. A survey of curve and surface methods in CAGD. *Computer Aided Geometric Design*, 1(1):1–60, 1984.